SPAWAR
Systems Center
PACIFIC

TECHNICAL REPORT 3043
September 2016

Radio Frequency Propagation and Performance Assessment Suite (RFPPAS)

Amalia Barrios
Stephen Lynch, Ph.D.
Neil Gordon, Ph.D.
Earl Williams, Ph.D.

SSC Pacific
San Diego, CA 92152-5001

SSC Pacific
San Diego, California 92152-5001

K. J. Rothenhaus, CAPT, USN
Commanding Officer

C. A. Keeney
Executive Director

ADMINISTRATIVE INFORMATION

The work described in this report was performed by the Atmospheric Propagation Branch (Code 55280) and the Command & Control Technology & Experiment Branch (Code 53603), Space and Naval Warfare Systems Center Pacific (SSC Pacific), San Diego, CA. Funding for this Technology Transition project was provided by the Naval Innovative Science and Engineering (NISE) Program at SSC Pacific.

Released by
D. Tsintikidis, Head
Atmospheric Propagation Branch

Under authority of
P. Juarez, Head
Networks Division

The citation of trade names and names of names of manufacturers is not to be construed as official government endorsement or approval of commercial products or services referenced in this report.

SB

EXECUTIVE SUMMARY

The Radio Frequency Propagation and Performance Assessment Suite (RFPPAS) is a 2-year effort funded under Space and Naval Warfare Systems Center Pacific's (SSC Pacific) Naval Innovation Science & Engineering (NISE) Technology Transition (TT) Program.

The objective of the RFPPAS project is to create thread-safe software modules and associated APIs from models and algorithms within the Advanced Refractive Effects Prediction System (AREPS). In a nutshell, the RFPPAS "cannibalizes" an operationally fielded tactical decision aid (TDA) for predicting radio frequency (RF) sensor performance, and then updates and improves its components to deliver fast, cloud-based, RF modeling performance on demand.

This software re-engineering effort will enable immediate integration of RFPPAS modules into PMW-120's program of record (PoR), the Naval Integrated Tactical Environmental System (NITES)-Next, as well as other new and existing software tools that rely on AREPS components. In addition, HSI and data management concepts were used to develop new databases and methodologies for creating decision aids, from large volumes of data and for multiple emitter/receiver(target) scenarios. Finally, a preliminary investigation was conducted into new concepts in multi-dimensional data visualization, using virtual reality technologies.

ACRONYMS

AOI	Area of Interest
API	Application Program Interface
APM	Advanced Propagation Model
AR	Augmented Reality
AREPS	Advanced Refractive Effects Prediction System
AWS	Aegis Weapon System
BEMR	Battlespace Exploitation of Mixed Reality
CANES	Consolidated Afloat Networks and Enterprise Services
CFSR	Climate Forecast System Reanalysis
C-ISR	Counter-Intelligence, Surveillance, and Reconnaissance
CNR	Clutter-to-Noise Ratio
CPU	Central Processing Unit
EDC	Evaporation Duct Climatology
EREPS	Engineer's Refractive Effects Prediction System
GPU	Graphics Processing Unit
HF	High Frequency
HSI	Human-Systems Integration
IRI	International Reference Ionosphere
ISR	Intelligence, Surveillance, and Reconnaissance
LSO	Landing Signals Officer
METOC	Meteorological and Oceanographic
MoE	Measures of Effectiveness
NASA	National Aeronautics and Space Administration
NAVSLaM	Navy Atmospheric Vertical Surface Layer Model
NCEP	National Center for Environmental Prediction
NGEN	Next Generation Enterprise Network
NISE TT	Naval Innovation Science & Engineering Technology Transition
NITES	Naval Integrated Tactical Environmental System (NITES)
NN	Naval Integrated Tactical Environmental System (NITES) - Next
NVIS	Near Vertical Incidence Skywave
NWP	Numerical Weather Prediction
OGC	Open Geospatial Consortium
OWF	Ozone Widget Framework
PCS	Propagation Condition Summary
PMW-120	Program Manager, Warfare - 120

PoD	Probability of Detection
PTH	Pressure, Temperature, Humidity
RAM	Random Access Memory
RCS	Radar Cross Section
RF	Radio Frequency
HRFP	Historical Radio Frequency Performance
RFPPAS	Radio Frequency Propagation and Performance Assessment Suite
SCNR	Signal-to-Clutter-Plus-Noise Ratio
SNR	Signal-to-Noise ratio
SSC Pacific	Space and Naval Warfare Systems Center Pacific
TDA	Tactical Decision Aid
VR	Virtual Reality
2-D	Two Dimensional
3-D	Three Dimensional

CONTENTS

Figures

Tables

1. INTRODUCTION

The Advanced Refractive Effects Prediction System (AREPS) is a Microsoft® Windows-based, thick-client software application that directly transitions to the currently fielded NITES-IV. NITES-Next (NN) is the follow-on from the Navy's legacy thick client NITES-IV system to a modern, web-based, Open Geospatial Consortium (OGC) compliant, Ozone Widget Framework (OWF) compatible with the U.S. Navy Enterprise IT architecture (Navy Tactical Cloud both afloat (CANES – Consolidated Afloat Networks and Enterprise Services) and ashore (AWS – Aegis Weapon System, NGEN – Next Generation Enterprise Network). The motivations for providing the NN Program Office with the RFPPAS of computational modules as thread-safe application program interface (API) plug-ins are to (1) reduce the overall cost of software development when the RF performance capabilities, provided by the AREPS models and algorithms are scheduled for NN integration, (2) maintain quality control and configuration management of the SSC Pacific-developed propagation models and algorithms, and (3) maintain the subject-matter expertise within the Atmospheric Propagation Branch at SSC Pacific for long-term maintenance and support.

The project is a 2-year funded program with supplemental external funding by PMW-120, the primary beneficiary of this effort. Results of the effort include:

1. 32-bit and 64-bit thread-safe Microsoft® Windows and Linux® modules of the post-processing algorithms determining the measures-of-effectiveness (MoE)
2. 32-bit and 64-bit thread-safe modules of three RF propagation models within AREPS (Advanced Propagation Model [APM], three-dimensional [3-D] ionospheric ray trace, tropospheric ray trace),
3. Propagation condition summary display templates
4. A historical RF performance database
5. Preliminary concepts for visualizing RF propagation modeling data using 3-D virtual-reality (VR) technologies.

2. PROPAGATION MODELS

2.1 ADVANCED PROPAGATION MODEL (APM)

The APM calculates propagation loss as RF energy propagates through a laterally heterogeneous atmospheric medium where the index of refraction is allowed to vary both vertically and horizontally, and is valid for frequencies from 2 MHz to over 94 GHz. The APM can accommodate propagation paths over sea water, land, and a combination of both, representing paths over coastal areas.

At the start of the RFPPAS effort, the APM existed as Fortran 95 legacy code with common blocks used for global variables throughout the model. This inherently prevented thread-safe execution of the library. The APM was also provided not as a single called procedure (function or subroutine), but as a series of several called procedures, making integration by a third-party developer more complicated.

In updating the underlying source code, a series of modifications were performed:

1. The entire source code was rewritten and updated to Fortran 2003/2008 to take advantage of object-oriented and advanced programming features in the modern Fortran language

2. All common blocks were removed and global variables were combined into various derived types, where the derived types are now passed to procedures as arguments
3. All procedures exposed to the developer are now combined into one single callable procedure, with minimal arguments, for easier integration
4. All constants (parameter types in Fortran) used throughout the code were combined into a single module for easier reference
5. Many utility and simple procedures were combined into a single module for ease of maintenance and supportability.

The APM model is now accessed via a single callable procedure, `apmrun`, and is thread-safe. This makes it easier to integrate and execute in a scalable, multi-process environment, as will be required for automated batch runs across a range of input parameters (see discussion of Figure 2 below). Its implementation is conceptually simple in that all input variables are passed to the model via a single derived type and all outputs are returned through a single derived type. The syntax is as follows:

```
call apmrun(apmin, apmout, ierror),
```

where `apmin` is the derived type containing all input variables required in order for a complete APM calculation, and `apmout` is the derived type containing all output variables returned to the calling application. The scalar variable, `ierror`, is returned with a non-zero value if invalid input data is found, or should an error occur with internal computations.

A list of the general input information required for a single APM run is listed in Table 1.

Table 1. Required input information for the APM.

Environment	
1	Height-varying refractivity profiles. One or multiple range-varying refractivity profiles can be specified.
2	Height-varying gaseous attenuation rate profiles. One or multiple range-varying gaseous attenuation rate profiles can be specified.
3	Logical flag directing how the atmospheric environment will be handled when the range-dependent refractive information does not coincide with the specified maximum range calculation.
4	Surface wind speeds and their direction relative to boresight. One or multiple range-varying wind speed(s) and direction(s) can be specified.
5	Scalar indicating how extrapolation of the refractivity profiles (defined relative to mean sea level (MSL) will be handled when the propagation path extends to land areas below MSL.
6	Height- and range-varying terrain profile. This is optional, in which case, the propagation path is assumed to be entirely over sea water.
7	Range-varying land use/land cover (surface composition) types. Required only if a terrain profile has been specified.
8	Surface dielectric types. One or multiple range-varying surface dielectrics can be specified.
9	Logical flag directing how the terrain environment will be handled when the range-dependent terrain information does not coincide with the specified maximum range calculation.
RF System	
1	Transmitting frequency
2	Transmitting antenna height
3	Vertical and horizontal beamwidths
4	Antenna pointing elevation angle
5	Type of generic antenna pattern or specific antenna pattern values
6	Polarization
7	Pulse length
General	
1	Logical flag directing if surface clutter is to be computed.
2	Logical flag directing if loss due to troposcatter is to be computed.
3	The geometry of the calculation area – consisting of the minimum and maximum height, and maximum range.
4	The output resolution of the fixed-grid propagation loss and propagation factor values.
5	Specific terrain-following receiver heights for output of propagation loss and propagation factor values. This is optional.
6	User-specified parabolic equation (PE) parameters for fine control of the split-step PE algorithm. This is optional.
7	Random number generator seed.
8	Process or thread ID.

A list of the output information returned from a single APM run is listed in Table 2.

Table 2. Output information returned from the APM.

Propagation Loss/Factor	
1	One-way propagation factor computed at a height of 1.0 m above ground level (AGL).
2	Propagation loss and propagation factor at the user-specified fixed resolution grid.
3	Propagation loss and propagation factor at the user-specified terrain-following receiver heights.
4	Scalar value indicating the validity of the surface value of the propagation loss/factor. This is dependent on the polarization specified on input.
General	
1	The surface clutter cross section for each pulse length.
2	The surface clutter reflectivity coupled with the two-way propagation factor.
3	The maximum wind speed allowed for the specified input frequency.
4	Nine variables consisting of two arrays and seven scalars that are provided for informational purposes to assist in monitoring execution and debugging.

For a more detailed list of input and output variables, along with units and numeric bounds, see Barrios, 2016. A typical APM output illustrating propagation loss (color scale) vs. height and range, over seawater in the presence of a surface duct, is shown in Figure 1.

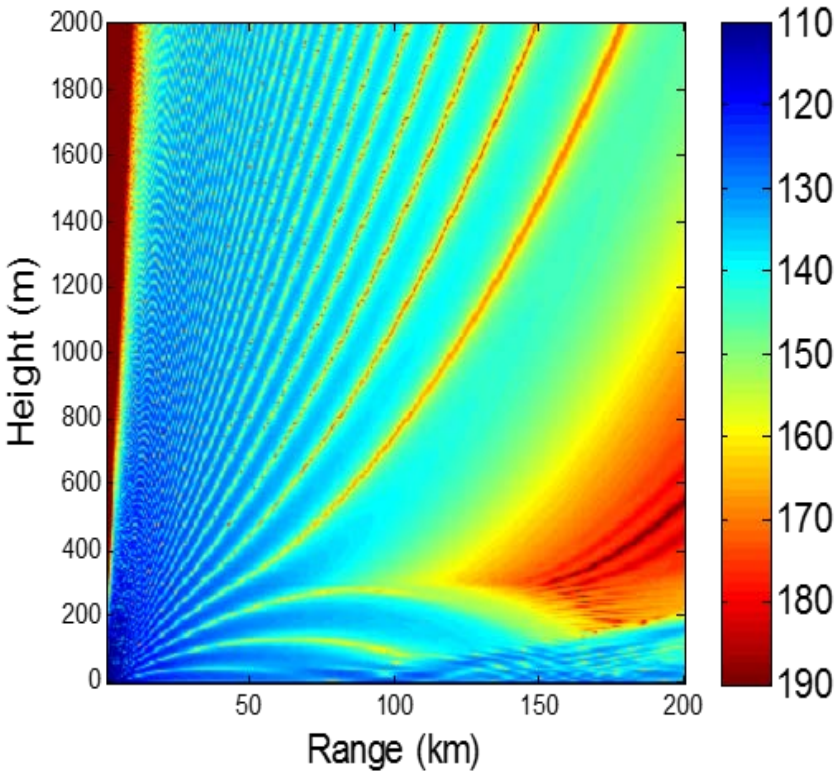

Figure 1. Propagation loss as a function of height and range from the APM.

.

As an example of the efficiencies gained with the updated APM module, Figure 2a displays an area detection map for a mock 3-D radar in the presence of surface ducting conditions against a target of a given size. The display is a typical operational application of an RF performance assessment of a shipboard radar, providing areas of vulnerability and detectability. To generate the display required APM to be executed 360 times (one APM run for each radial). Figure 2b shows the APM execution times before and after the update for this particular case. "Before – single thread" refers to the execution time, 814 seconds, of the APM version at the start of the RFPPAS effort running a single thread. "After – single thread" is the updated APM version, now thread-safe, but also running a single thread. Here the execution time was reduced to 581 seconds. Finally, "After – 4 threads" is the updated APM version, but now run using four threads, which reduced the overall execution time to 196 seconds. The computer platform in this test was a PC with the 64-bit Microsoft® Windows 7 (Service Pack 1) OS, a 4-core Intel Xenon CPU E3-1230 V2 processor running at 3.30 GHz, and 12 GB of RAM.

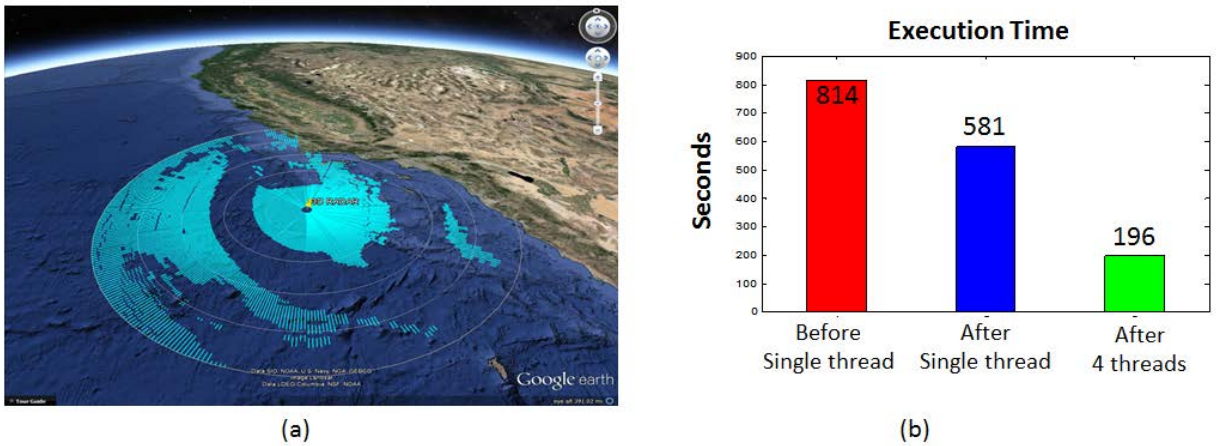

Figure 2. (a) RF performance assessment, and (b) corresponding execution times for APM before updates, after updates, and after updates executed with four threads.

2.2 TROPOSPHERIC RAY TRACE

The tropospheric ray trace model is taken from the AREPS predecessor, "Engineer's Refractive Effects Prediction System (EREPS) (Patterson et al., 1994), and is largely unchanged except for the additional ability to accommodate terrain paths. The ray trace equations are based on small angle approximations to Snell's law. They provide a qualitative summary of ray trajectory, or more specifically, the trajectory of the perpendicular to the wavefront, for any RF emissions propagating within the troposphere. The model is frequency-independent, as there is no computation of field strength but simply serves as a quick, but useful, illustration of how RF emissions will be affected by the tropospheric and terrain environment along a path. Although field strength is not computed, the density of rays along the path can provide a qualitative look as to areas of high or low signal strength. Additional information such as the altitude-error along the path is also determined. This represents the height difference of the ray relative to its height if propagating through a standard atmosphere. For a detailed description of the tropospheric ray trace algorithm, refer to Patterson et al., 1994.

Similar to the APM, a series of modifications were performed to the underlying ray trace source code:

1. All source code was converted from Visual Basic 6.0 to Fortran 2003 and made thread-safe
2. All procedures exposed to the developer are now combined into one single callable procedure, with minimal arguments, for easier integration
3. Many utility and simple procedures were combined into a single module for ease of maintenance and supportability.

The tropospheric ray trace model is now accessed via a single callable procedure, `TraceAllRays`. Its implementation is conceptually simple in that all input variables are passed to the model via two derived types, one for the specific atmospheric conditions desired, and one for standard atmosphere conditions, with all outputs returned through a single derived type. The syntax is as follows:

```
call TraceAllRays(rayIn, rayInStd, rayOut, ierror).
```

Similar to the APM, the scalar variable, ierror, is returned with a non-zero value if invalid input data is found, or should an error occur with internal computations.

A list of general input information required for a single execution of the tropospheric ray trace model is listed in Table 3.

Table 3. Required input information for the tropospheric ray trace model.

Environment	
1	Height-varying refractivity profiles, as well as a range-independent standard atmosphere profile. One or multiple range-varying refractivity profiles can be specified.
2	Height- and range-varying terrain profile. This is optional, in which case, the propagation path is assumed to be entirely over sea water.
General	
1	Transmitting antenna height.
2	The geometry of the calculation area – consisting of the minimum and maximum height, and maximum range.
3	Minimum and maximum launch angles and the number of rays to be traced.
4	The number of ray segments expected for each ray (used for array sizing).
5	Flag indicating if determination of the altitude error is to be performed.
6	Process or thread ID.

A list of output information returned from a single execution of the tropospheric ray trace model is listed in Table 4.

Table 4. Output information returned from the tropospheric ray trace model.

Ray Information	
1	Heights and ranges of the ray trajectory for all rays traced.
2	Altitude error relative to standard atmosphere for all rays (if specified on input).
3	Propagation angle at the end of each ray segment for all rays.
4	The grazing angle (angle of reflection from the surface), if applicable, for all rays.

A typical output from the tropospheric ray trace model is shown in Figure 3, where multiple rays are traced from a surface-based emitter over a coastal path. The emitter is located over water and radiating inland towards the coastline, with the terrain represented in brown. The atmosphere is a surface-based duct and the color sections of any one ray represent the height difference of the ray relative to the height it would be at that same range under standard atmosphere conditions, for the same launched ray angle.

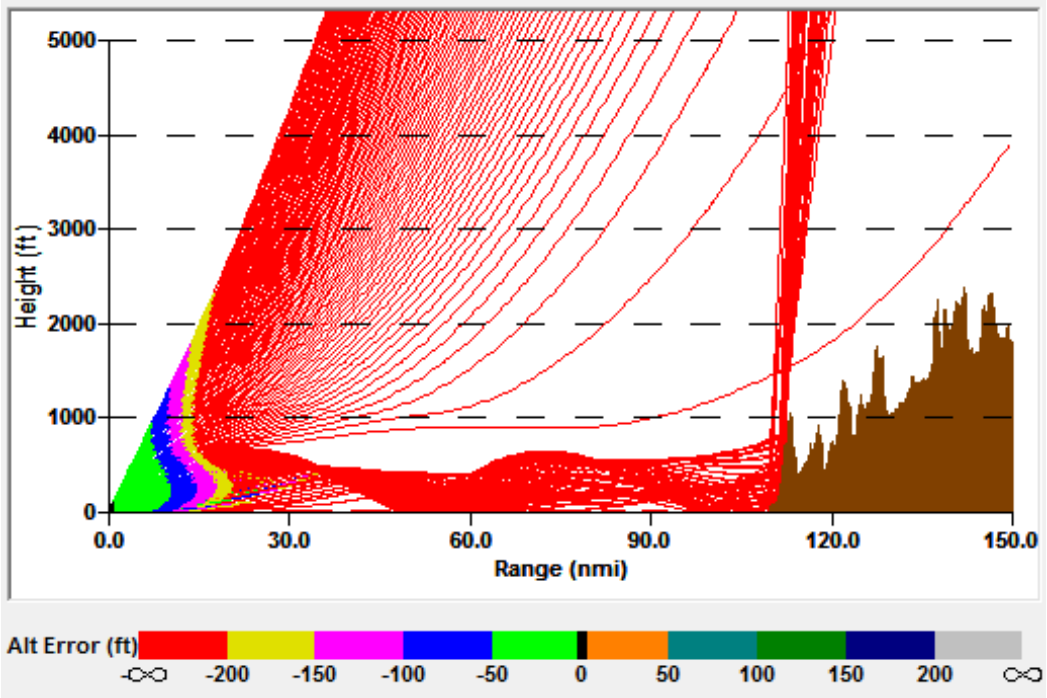

Figure 3. Tropospheric ray trace displaying multiple rays traced in the presence of a surface-based duct over a mixed land-sea path, along with altitude errors.

2.3 IONOSPHERIC RAY TRACE

The 3-D ionospheric ray trace, or IonRayTrace, is a Hamiltonian optics-based ray trace program for use in HF propagation predictions. The model is a heavily revamped (updated and reorganized) version of the original Jones-Stephenson Fortran model (Jones and Stephenson, 1975), that resides in the AREPS. The central kernel traces rays through a three-dimensionally varying medium, including anisotropic and dispersive effects. The current version is written with Fortran 2003 standards, and has been built to address myriad applications efficiently, including many-node point-to-point (e.g., communications networks), illumination (e.g., radar), hybrid (e.g., illumination with scattering), and computationally intensive (e.g., inverse problem) applications.

Differences between the updated and original versions of the IonRayTrace are too many and too significant to describe fully here. Common blocks were eliminated in all but the International Reference Ionosphere (IRI) background environment estimation module. Additionally, the model is thread-safe and parallelized, and can be executed on multiple platforms through OpenMP and OpenMPI, making it well suited for use in inverse and other computationally intensive problems (see Figure 4). As of writing this report, further development continues towards running the IonRayTrace

on GPU accelerators. Finally, additional methods which utilize the ray trace output to estimate channel response were developed.

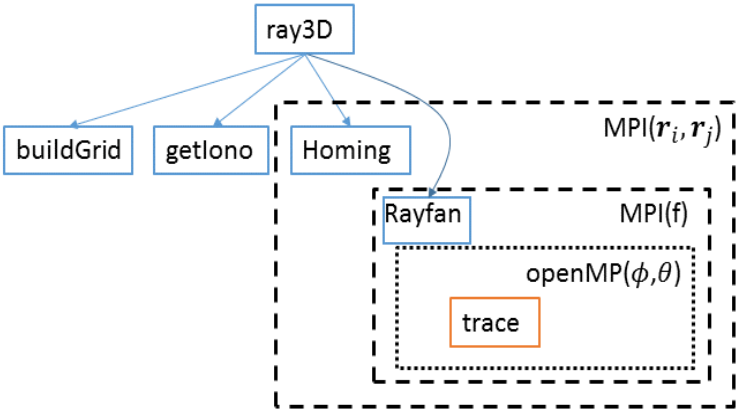

Figure 4. Overall workflow of the current IonRayTrace model, including MPI and openMP organization.

Major changes have resulted in input and output formats that are nearly entirely different from those in the previous versions (Lynch, 2014; Ferguson and Shellman, 1993). Additionally, an API was developed that utilizes ISO_C_Bindings to enable seamless integration into other environments such as Python.

2.3.1 Electron Density (Plasma Frequency)

The IonRayTrace can be run using three different types of environment, including the International Reference Ionosphere (IRI) (Bilitza, 2001), arbitrary gridded free electron density volume, or a handful of canonical models. This enhanced ability to utilize arbitrary ionosphere environments is central to inverse estimation applications. All inputs and outputs are accessible through a single, Fortran-like function call to IonRayTrace, e.g., from within Python. Table 5 lists the required inputs to run the IonRayTrace model. Note that this list of inputs does not reflect the full list of variable names, as most input variables are attributes to defined Fortran types—the full description of these types and how the API handles these is discussed in a separate document. Table 6 contains additional inputs that may be required, depending on the values of the parameters in Table 5.

Table 5. Required inputs for using the IonRayTrace model.

Variable	Type	Allowed values
Scenario: Network, Illumination, or IRI environment only	Integer	1 (Network), 0 (Illumination), -1 (IRI)
Model types: electron density, magnetic field, and absorption	Thee-vector integer	$(0, \pm 1, \pm 2, \pm 3)$ electron density, $(0\text{-}2)$ magnetic field, $(0\text{-}3)$ absorption
Transmitter location(s): Latitude (deg N+), longitude (deg E+), altitude above mean sea level (km) for all NTx transmitters	3 x NTx array float	[-90.0, 90.0], [-180.0, 180.0] or [0.0, 360.0] ≥ 0.0
Receiver location(s): range (km), bearing (deg from geodetic north), altitude (km)	3 x NRx float array	> 0.0 km, any real number, ≥ 0.0 km
Quality: Whole network and reciprocal propagation (Scenario == 1), or azimuthal fan half-width (deg) and step size (deg)	Two-vector float	$\geq 0.0, \geq 0.0$
Date: Date and UTC to run IonRayTrace, needed only for using IRI 2012	Four-vector integer	[YYYY, MM, DD, hhmm]
Max counts: maximum hops and maximum points stored along path	Two-vector integer	$> 0, \geq 0$
Frequencies: List of Nfreq frequencies (MHz) for tracing rays	Nfreq float	[2.0, 30.0] MHz
Polarization: Ordinary, extraordinary, or both	Integer	1 (O), -1 (X), 0 (both)
Solar-terrestrial indices: Kp Index, month-averaged 10.7-cm solar flux (S.F.U.), and gyro frequency (MHz)	Three-vector float	[0.5, 9.0], [0.0, 400.0], > 0.0

In cases where the IRI 2012 is used, a list of dates and times must be provided, as well as node locations and geo-terrestrial parameters for each time step. The IonRayTrace uses the node locations at each time step to build the grid, by first finding the maximum distance between two nodes. That maximum-distance great circle path defines the x-coordinate. The grid width is then determined by the maximum distance of all remaining nodes to the x axis. Note that in illumination cases the maximum range is one of the inputs, and the maximum y distance is computed from the ray fan half-width and maximum range. The resulting grid spacing is 200 km, and the grid contains a buffer "curtain" around each edge of at least 400 km from any node. Once the IonRayTrace defines this grid, it runs the IRI at all its points for each time step. In this way the same interface is used for both the IRI and arbitrary gridded environments. There are no plans to further modify the IRI code, which is maintained separately by NASA, as doing so is outside the scope of this project.

In cases where a pre-defined free electron density volume is used (for instance, in inversion problems), the input environment data must be of equal *xy* spacing, in part because the program interpolates the grid using cubic splines. While the vertical spacing can vary with altitude, it must be the same at every *xy* point.

Finally, the user can set the IonRayTrace to run using the canonical models still included in the code, including Chapman layer and Equatorial Bulge models. For more information about these models, see Jones and Stephenson (1975).

2.3.2 Magnetic Field and Absorption (Collision Frequency)

In addition to the various electron density environment options, the user can choose from several models for the background magnetic field, as well as the collision frequency model used. The background magnetic field can be estimated one of three ways:

1. The gyro-frequency decreases with the distance from earth's center cubed
2. An earth-centered dipole
3. Model of the earth's magnetic field based on harmonic analysis.

Similarly, collision frequency can be estimated one of five ways, each requiring different inputs from the user.

1. Constant everywhere
2. Varies exponentially with altitude
3. Varying as the sum of two exponentials with altitude
4. A double Gaussian bump
5. Tabled collision frequency values

In cases 1 through 4, the IonRayTrace uses default values listed in Table 6 if the user does not provide values.

2.3.3 Environment Types

The three-vector of model types [*Xtype*, *Ytype*, *Ztype*] determines how the IonRayTrace will compute the background free electron density (in frequency units), magnetic field, and collision frequencies. If *Xtype* is 0, the IonRayTrace reads in the user-specified gridded electron density data. If |*XType*| = 1, IonRayTrace first builds a gridded box containing all the node locations, plus a minimum 400.0-km buffer on each edge, and calls the IRI 2012 with the date and geo-terrestrial data to compute the vertical electron density profiles at each grid point. *XType* values of 4, 5, and 6 indicate Chapman layer, equatorial bulge, and variable-scale-height Chapman layer profiles, respectively. If *XType* is negative, the IonRayTrace computes a wave-like perturbation to the electron density field. For |*XType*|>3 and perturbation cases, the requisite parameters specifying these profile types must then be specified (see Table 6).

Table 6. Profile types for the IonRayTrace.

Parameter	Type	Allowed or default values
Chapman: reference height h_m (km), scale height h_s (km), ripple amplitude *a* (natural units), ripple wavelength *b* (km), gradient amplitude *c* (natural units), tilt *e* (rad^{-1}), alpha	Seven-vector float	≥ 0.0
Variable Chapman: max height h_m(km), height exponentχ (natural units), reference frequency f_c (MHz)	Three-vector float	≥ 0.0
Perturbation: wavelength (km)		≥ 0.0
Exponential collision frequency: Scale height (km/MHz), reference height (km), and reference collision frequency (MHz)	Three-vector float	≥ 0.0
Dual exponential collision frequency: Scale height 1 (MHz/km), ref. height 1 (km), ref. collis. freq 1 (MHz), scale height 2, ref. height 2, ref. collis. freq. 2	Six-vector Float	≥ 0.0

2.3.4 Scenario Types

The IonRayTrace is built to run efficiently in either Illumination or Network modes. Most applications can be addressed effectively using one or both of these modes.

2.3.4.1 Illumination

Illumination mode traces rays through a given volume. Individual rays are varied in vertical and azimuthal angles, frequency, and polarization mode, according to user input. Wave front properties calculated along these ray paths can then be used to estimate HF signal parameters over a given area or at given node locations.

2.3.4.2 Network

The Network mode performs an iterative search for "eigenrays," rays that link a pair of nodes, at user-specified frequencies.

The IonRayTrace previously included the capability to conduct an iterative search (homing) for eigenrays that intersected the receiver height at ranges that fell within some tolerance window of the receiver range. While the ray trace program is three-dimensional, the homing was essentially two-dimensional (vertical take-off angle and altitude), and it was common to find eigenrays that had deviated significantly in azimuth from the great circle arc between the nodes, and it was common for the resulting eigenrays to intersect at points hundreds of km away from the receiver node, even though the range tolerance criterion was met. So the updated IonRayTrace includes a 3-D (vertical and azimuthal angles, plus altitude) homing algorithm, in addition to the previous 2-D capability.

To use CPU time most effectively, the IonRayTrace computes minimum and maximum take-off angles from the great circle distance between the node pair, and the specified maximum number of hops, as well as the lowest altitude in the gridded environment at which plasma frequency is $\geq$ 0.1 MHz (for take-off angle minimum), and maximum F-layer peak altitude within the gridded area

for maximum take-off angle. If two-dimensional (2-D) homing mode is selected, only a single vertical ray fan will be computed. For 3-D homing, a 2-D initial ray fan is computed bounded by these minimum and maximum vertical angles, and $\pm 5°$ about the bearing from the transmit node to the receive node. Following this initial ray fan, the IonRayTrace conducts an iterative search on each mode, decreasing the initial angle spacing in subsequent 2-D ray fans until the area of the Delaunay triangle containing the receive node falls below $2.5 \times 10^{-5}\ R^2$, where R is the great circle range between transmit and receive node locations.

2.3.5 Ionogram

One important previous application for which the IonRayTrace was used was computation of oblique ionograms, or estimates of group and phase delays between two arbitrarily placed nodes as a function of frequency. In making this computation the IonRayTrace previously defaulted to the homing mode at all frequencies between 2.0 and 30.0 MHz, in 1.0-MHz steps. While it was possible to alter this configuration to include different frequency interval sizes or different upper or lower limits, doing so required recompiling the module, which is neither practical nor even accessible for most users. However, enabling the program to find rays at an arbitrary list of frequencies allows the user to investigate portions of the HF spectrum in fine grain, while not sacrificing computational resources to probe portions of the spectrum where there is little variation with frequency. The change in inputs to variable lists achieves this flexibility, as well as the ability to compute ionograms between more than two node locations in one run. Overall, the current configuration can complete ionogram estimates faster through parallelization. While the 3-D homing capability can potentially lead to more accurate results, as well as enable new areas of investigation in cases where horizontal refraction affects propagation paths supported between two nodes; improved accuracy in the ray trace results always depends on improved estimates of the background-free electron density environment and magnetic field.

2.3.6 IonRayTrace Output

The IonRayTrace can return up to three types of data—it will always return at least one type. The first is the environmental (ionosphere electron density) data, including latitude and longitude of the grid points, the vertical profiles of electron density at each grid point, as well as the peak plasma frequencies for the F2, F1, and E layers (foF2, foF1, and foE, respectively); and the heights at which this occurs: hoF2, hoF1, and hoE, respectively.

Second, the IonRayTrace can return HF wave and scenario information at all the points where the rays intersect the receiver altitude, including Transmit and Receive node numbers, frequency, O/X mode, number of reflections from the surface along the path leading to each point, initial and incident elevation and azimuthal/bearing propagation directions, latitude and longitude of points of incidence, deviation in azimuth from the great circle path traced from initial bearing, group, phase, and geometric path lengths; Doppler shift, absorption losses, initial and incident ray-tube cross sections, complex transverse and longitudinal polarization, and apogee.

The ray tube cross section is computed one of two ways, depending on whether the homing search was conducted over azimuthal and elevation angles, or elevation only. In the case of the former, the cross-sectional areas are πab, where a, b are the lengths of the semi-minor and semi-major axes of the Steiner circum-ellipse of the Delaunay triangle formed by the ray path points immediately

surrounding the receiver location. The cross-sectional areas are the criteria quantities for continuing the homing search: when they are sufficiently small, the search is completed. In the case of the vertical angle search only, the cross-sectional parameter is the width of the cross section only ($dR \sin \alpha$, where α is the incident elevation angle and dR is the difference in range of the ray points bracketing the receiver range), as it assumes cylindrical azimuthal spreading.

Finally, if the maximum path point count is greater than 0, the IonRayTrace returns altitude, range, bearing angle and deviation, latitude, longitude, and complex transverse and longitudinal polarization along each path, as well as group, phase, and geometric path lengths at the end point; and initial bearing and elevation propagation angles.

2.3.7 Application Examples

Figure 5 is an example result of the Network mode from the IonRayTrace. For a sample network, the IonRayTrace predicts single- and multi-hop paths over most of the HF band (7.0 to 18.0 MHz) to support a network consisting of afloat and shore-based nodes, with long-haul and Near Vertical Incidence Skywave (NVIS) links. Heat maps depicting E- and F2- layer peak plasma frequencies are displayed on the 3-D graphic boundaries, as well as floating through the volume.

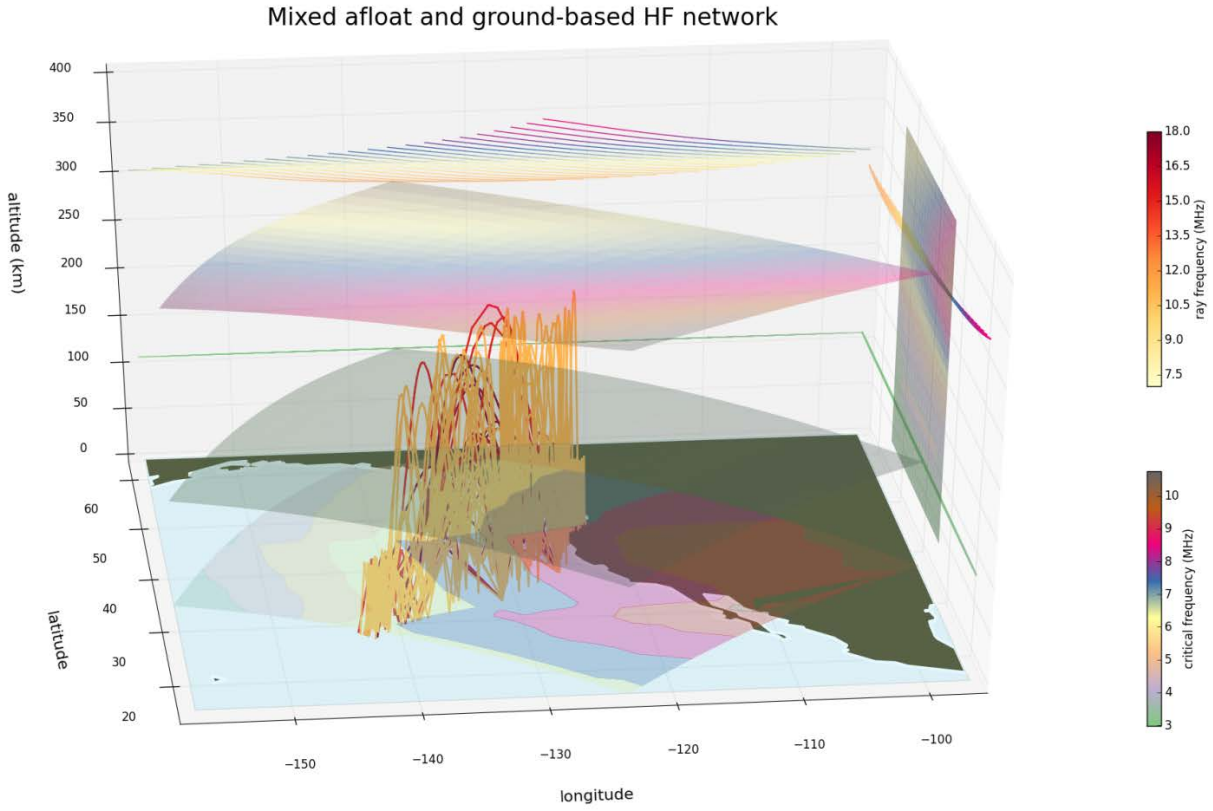

Figure 5. The IonRayTrace paths found using homing over vertical and azimuth at several frequencies for a mixed communications network consisting of afloat and shore-based nodes. The background environment was estimated using IRI, 2012. The heat maps indicate frequencies of the E and F2 layers. Projected on the surface are the maximum plasma frequency over the grid, and the projection on the eastern boundary of the graphic is a vertical slice through the ionosphere volume.

An example result of the illumination mode of execution from the IonRayTrace is shown in Figure 6.

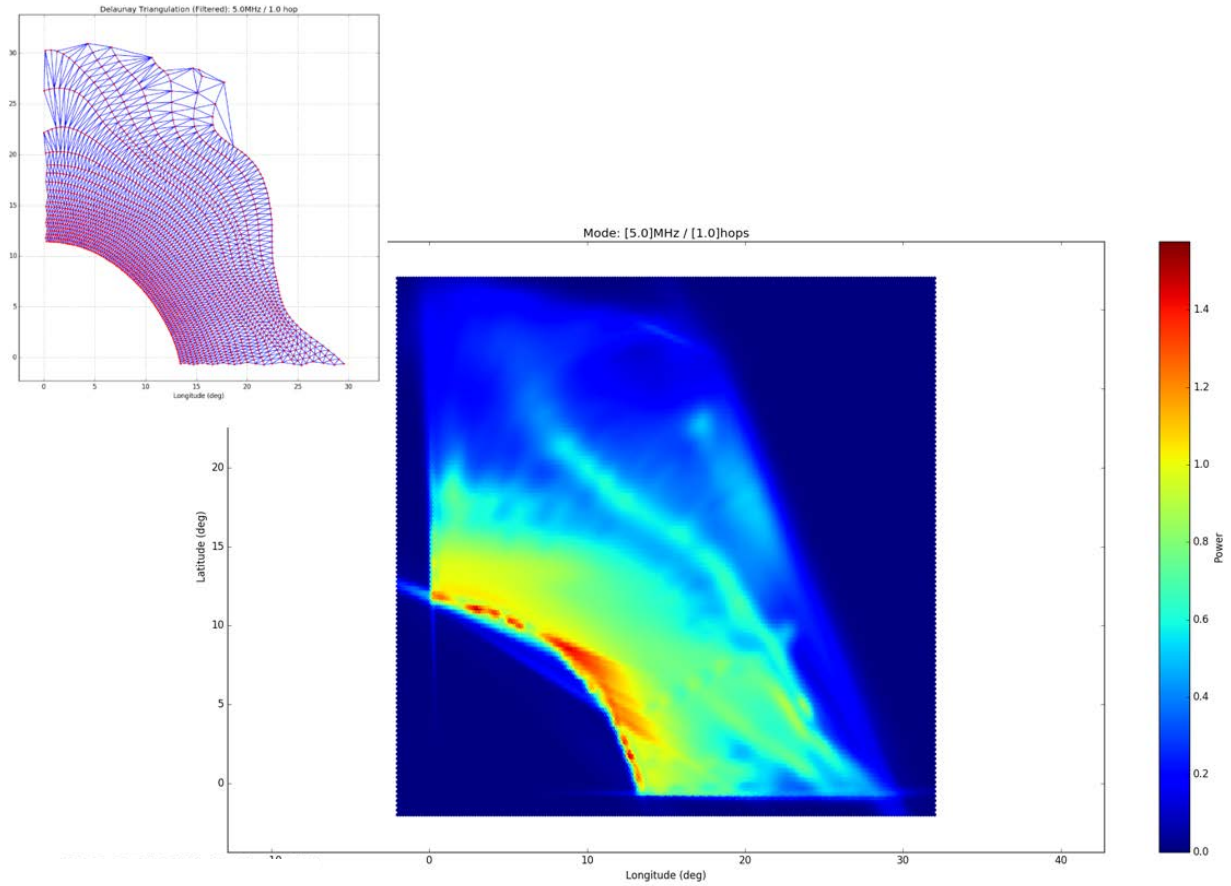

Figure 6. An example of IonRayTrace's results for an illumination application. Delaunay triangulation (inset) used for sorting ray points by mode type and phase path difference, for use in computing covariance eigenvectors for Gaussian ray bundle-based estimation of incident intensity.

3. MEASURES OF EFFECTIVENESS (MOE)

The post-processing algorithms within the AREPS are those algorithms and models that compute a meaningful metric for eventual display to the warfighter, based on the propagation loss or field strength determined from the propagation models. Parameters that are computed within the MoE module are

1. Electric field strength in dBV/m, E
2. Received power in dB, P_r
3. Electronic Support Measures (ESM) received power in dB, P_{rESM}
4. Signal-to-noise ratio (SNR) or signal-to-clutter-plus-noise ratio (SCNR) in dB
5. Probability of detection, PoD
6. Minimum detectable radar cross section (RCS) in dB, σ_{min}.

All propagation loss or propagation factor computations within the APM are based on one-way propagation. However, whether the emitter is a radio or radar will dictate how the computation of received power is performed.

3.1 ELECTRIC FIELD STRENGTH

The electric field strength is defined by

$$e^2 = \frac{Z_o 4\pi\, p_r}{\lambda^2}, \tag{1}$$

where Z_o is a constant representing the free space impedance with a value of 120π, p_r is the power form of the received power, and λ is the wavelength. The received power at some range R is

$$p_r = \frac{p_t g_t \lambda^2 F^2}{(4\pi R)^2}. \tag{2}$$

Here, p_t is the transmitted power, g_t is the gain of the transmitting antenna, and F is the pattern propagation factor computed from the APM. Combining Equations (1) and (2) and writing quantities in dB form gives

$$E = -12.78 + P_t + G_t + 20\, log_{10}(f_{MHz}) - L_{APM}, \tag{3}$$

where the constant is a combination of fixed constants plus the conversion factor from wavelength to frequency, the power is provided in watts, making P_t in units of dBW, f_{MHz} is frequency in MHz and L_{APM} is the propagation loss computed from the APM:

$$L_{APM} = 20\ log_{10}\left(\frac{4\pi R}{\lambda}\right) - 20\, log_{10} F. \tag{4}$$

The first term in Equation (4) is the free space loss in dB. The electric field strength provided in Equation (3) is in dBV/m. To compute E in dBμV/m simply add 120.

3.2 RECEIVED POWER

The received power is determined slightly differently depending on the system being modeled. The received power for a communications system, a bistatic arrangement where the transmitter and receiver are not co-located and one-way propagation only is required, is determined in dBW as

$$P_{r(com)} = P_t + G_t + G_r - L_{APM} - L_{sys} - L_{cp}. \quad (5)$$

The transmitted power is defined as in Equation (3), in dBW, and the gains of the transmitting and receiving antennas are G_t and G_r, respectively, also in dB. The loss from APM, L_{APM} is defined in Equation (4), and L_{sys} refers to the total system losses (line losses, filter mismatch loss, etc.) for both transmit and receive systems. Finally, L_{cp} is the cross polarization loss, defined as

1. L_{cp} = 0 dB if both the transmitter and receiver have the same polarization
2. L_{cp} = 3 dB if one of the terminals are circularly polarized
3. L_{cp} = 15 dB if one terminal is horizontally polarized and the other is vertically polarized.

For an ESM receiver system, the bistatic geometry is still applicable and Equation (5) is identical, however, the quantities are defined differently. In this case the received power is defined as

$$P_{r(ESM)} = P_t + G_t + G_{r(ESM)} - L_{APM} - L_{sys(ESM)} - L_{cp}. \quad (6)$$

The received power $P_{r(ESM)}$ is in dBW and P_t is the transmitter power, in dBW, of the emitter, whether it be a radar or communication system. The receiving antenna gain $G_{r(ESM)}$ is now the gain, in dB, of the ESM antenna and the system losses $L_{sys(ESM)}$ refer to all losses associated with the receive system only. Presumably any losses or other emitter parameters are unknown, however, if they become known these can be added to the above equation. All other terms in Equation (6) are defined as in Equation (5).

To compute the received power **for a radar system** we begin with the simple form of the radar range equation (Skolnik, 2008):

$$p_r = \frac{p_t g_t g_r \lambda^2 \sigma F^4}{(4\pi)^3 R^4 l_{sys}}. \quad (7)$$

Most of the parameters are defined similarly as in Equation (2), however, in the radar case, transmit and receive antennas are co-located or may be identical, hence the additional g_r term. Two additional terms are the target RCS, σ, and the total system losses (in power form), l_{sys}. In the radar case, the power to the target and that reflected back toward the receive antenna is what is computed in Equation (7). Therefore, we determine the two-way propagation loss to compute the received power, reflected in the F^4 and R^4 terms. In dB form, Equation (7) becomes

$$P_r = -38.55 + P_t + 10\,log_{10}(f_{MHz}^2 \sigma) + 2G - L_{sys} - 2L_{APM}. \quad (8)$$

Here again, the constant is a result of combining the constants in Equation (7) with other conversion factors. Transmit and receive antenna gains are assumed identical in the above equation and σ is in units of m^2. All remaining terms are defined as in Equations (4) and (5).

3.3 SIGNAL-TO-NOISE RATIO (SNR)

The *SNR* for any emitter is computed simply as

$$SNR = P_r - P_n \,, \tag{9}$$

where all quantities are in dB. For a communication or ESM system the received power, P_r, is defined as in Equations (5) and (6), respectively. The noise power, P_n, in dB, is defined as

$$P_n = -203.98 + 10\,log_{10}\,B + N_f. \tag{10}$$

The constant comes from the term $10\log_{10}(kT^o)$, where k is Boltzmann's constant (1.38×10^{-23}) and we assume a reference temperature of 290 K. B is the bandwidth, in Hz, of the receive system and N_f is the noise figure in dB.

For a radar system, pulse length (or pulse width) is typically provided as part of the system specifications rather than bandwidth. In this case, the noise power is computed as

$$P_n = -143.98 - 10\,log_{10}(\tau) + N_f, \tag{11}$$

where τ is the pulse length in microseconds. To compute *SNR*, simply use Equations (8), (9), and (10), or (11), depending on the particular RF system.

3.4 SIGNAL-TO-CLUTTER-PLUS-NOISE RATIO (SCNR) AND CLUTTER-TO-NOISE RATIO (CNR)

Computing the *SCNR* can be done in one of several ways. The most concise method can be done by modifying the simple form of the radar range equation, Equation (7), to contain all surface clutter information. However, the procedure described here is outlined for clarity and to provide an easy means to compute the *CNR*, which may also be desired as a separate quantity.

We begin by first determining the received power at the radar due to clutter alone. In Equation (7), if we replace the target RCS, σ, with σ_c, the surface clutter cross section, and F with F_c, which now represents the propagation factor at the surface, we can write the received clutter power, P_c, as

$$P_c = 16.57 + P_t + 10\,log_{10}\left(\frac{\sigma_c}{f_{MHz}^2 R^4}\right) + 2G - L_{sys} + 2F_{c(dB)}. \tag{12}$$

If you look carefully, Equation (12) is identical to Equation (8), when using the propagation factor form of the equation instead of the propagation loss, and replacement of σ_c and F_c. Here, it is explicitly written that $F_{c(dB)}$ is the dB form of the propagation factor (i.e., $F_{c(dB)} = 20\log_{10}(F_c)$). Two quantities that are output from the APM are σ_c in dB and $F_{c(dB)}$. Therefore, using Equations (11) and (12), the CNR can be computed from

$$CNR = P_c - P_n. \tag{13}$$

It is now a relatively simple procedure to determine *SCNR*, in dB, using Equations (8), (11), and (12):

$$\frac{S}{C+N} \equiv SCNR = 10\,log_{10}\left(\frac{p_r}{p_c + p_n}\right), \tag{14}$$

where the lowercase variables in parentheses are their respective quantities in power form, not in dB.

3.5 PROBABILITY OF DETECTION (POD)

For a given radar system, the PoD is dependent on many system-specific parameters, which include the probability of false alarm, dwell time, pulse length, and the type of internal processing of the radar, just to name a few. What is necessary to determine is the minimum SNR required, SNR_{min}, for detection for a given PoD value. Once SNR_{min} is determined, this is compared with the SNR computed from Equations (8), (9), and (11) to obtain the PoD in a heterogeneous environment against a real target. A full description of the PoD algorithm as used with the APM is not duplicated here but provided in Barrios (In progress).

3.6 MINIMUM DETECTABLE RCS

It naturally follows that the minimum detectable RCS is that which produces the minimum SNR required for detection, SNR_{min}. Using Equations (8) and (9), we can write the minimum detectable RCS, σ_{min} in dB, as

$$\sigma_{min} = 38.55 + SNR_{min} + P_I + L_{sys} - P_T - 20\,log_{10}\,f_{MHz} - 2G + 2L_{APM}, \quad (15)$$

where all parameters are defined as before and P_I represents the total noise, or interference, power defined as

$$P_I = 10\,log_{10}(p_c + p_n)\,. \quad (16)$$

4. PROPAGATION CONDITION SUMMARY DISPLAYS

Atmospheric ducting provides a means to induce greater-than-normal propagation of RF emissions within the troposphere, typically referred to as “enhanced propagation,” which can lead to detection or communication at ranges much greater than expected. Conversely, this can also lead to signal intercept or detection of blue forces by red forces at much greater ranges. Knowledge of where and when these features can occur in the atmosphere can aid in tactical or strategic planning for intelligence, surveillance, and reconnaissance (ISR) or counter-ISR (C-ISR) applications, and can also dictate when a more detailed RF performance assessment is required by running the propagation models described in Section 2.

As stated in Patterson and Barrios (2016), several meteorological conditions will lead to the creation of ducts. If these conditions cause a trapping layer to occur, such that the base of the resultant duct is at the earth's surface, a surface duct is formed. There are three types of surface ducts, based on the trapping layers' relationship to the earth's surface. First is a surface duct created from a surface-based trapping layer, referred to as a surface duct. Second is a surface duct created from an elevated trapping layer, commonly referred to as a surface-based duct. Third is a surface duct created by a rapid decrease of relative humidity immediately adjacent to the air–sea interface. This third type is referred to as an evaporation duct. In addition to surface ducts, there can also be an elevated duct in which the base of the duct occurs above the earth’s surface. A trapping layer refers to a height layer in which the refractivity gradient decreases with altitude, causing radiowaves to bend towards the earth’s surface.

The U.S. Navy obtains atmospheric, or weather, information from numerical weather prediction (NWP) forecasts that are typically performed over large-scale geographic areas with varying horizontal resolution. The propagation condition summary (PCS) displays are a means to visualize variations in refractive features and environmental conditions that may affect RF propagation over a NWP region.

The displays are not necessarily designed for operational meteorological and oceanographic (METOC) personnel, but for the non-METOC user, where little to no knowledge of environmental impacts on RF emissions is assumed. The displays include brief narratives to answer the question: "what does this refractive feature, or atmospheric condition, mean to me?" for the communications, cryptologist, radar, etc., operational personnel. The displays are intended to provide an *awareness* of propagation conditions that can significantly affect RF performance within an area of interest (AOI), not to provide specific detection range or probability of detection estimates, as no propagation model is executed in the generation of these displays.

4.1 DUCT MAP

The duct map displays areas containing surface ducts only (exclusive of evaporation ducts), elevated ducts only, and elevated plus surface ducts. This display provides an overall indication of the extent of anomalous propagation features present within the NWP region that may affect the majority of the RF spectrum for which the underlying propagation models are applicable.

For instance, in the example in Figure 7, the presence of "elevated ducts" over large areas may indicate that airborne emitters may be subject to enhanced propagation, and that aircraft (targets) may be vulnerable to detection at greater ranges. The extent (i.e., heights) at which elevated ducts or surface ducts occur is not explicitly indicated here, but can be viewed in conjunction with PCS displays described in Sections 4.2 and 4.4. This PCS display is provided as a "quick and dirty" indicator that a given region may warrant further investigation.

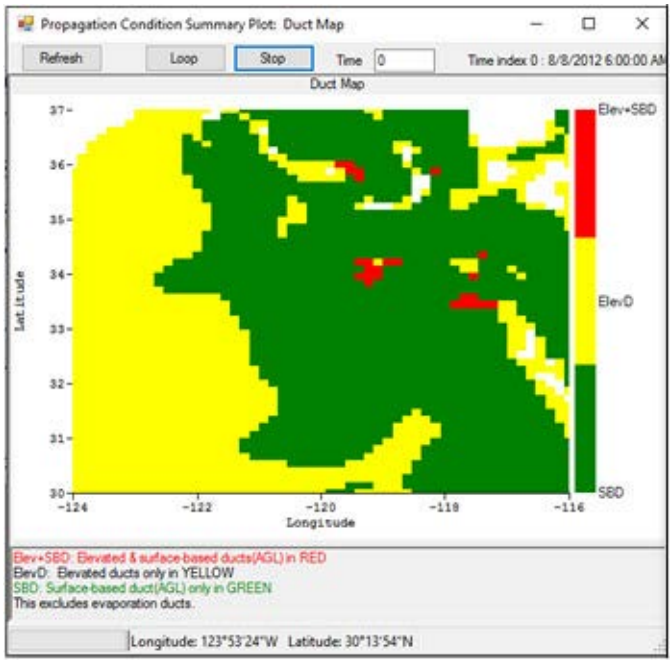

Figure 7. Duct map PCS display.

4.2 EXTENDED RANGE MAP – SURFACE EMITTERS

This PCS display shows areas where “surface ducts only” are present. This category includes larger surface ducts created by thermal inversion processes only (i.e., it excludes evaporation ducts). The contours represent the extent of the duct height from the surface. This indicates locations at which surface emitters, or more specifically, those emitter antenna heights below the duct height shown, may be subject to enhanced propagation for a particular latitude/longitude location, which is also stated in a general way by the narrative provided in conjunction with the graphic, as shown in the example in Figure 8.

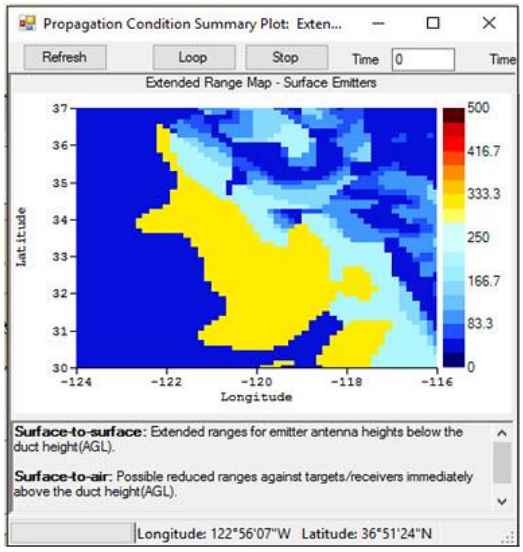

Figure 8. Extended range map-surface emitters PCS display. Colors represent duct heights in meters.

The particular effect that the anomalous propagation features induce on RF emissions are subject to transmitter/receiver geometries. As stated in the narrative in Figure 8, for surface-to-surface geometries (surface emitters against surface targets/receivers), if both terminal points are below the duct heights shown along any path, one can expect enhanced propagation—or equivalently, extended communications and detection ranges between the terminals. One of the significant impacts a surface-duct can induce on a surface emitter is a “radar hole” in which reduced coverage occurs for targets (or receivers) located just above the duct height, which is stated in the “surface-to-air” narrative. Surface ducts have minimal effect for air-to-air geometries.

Again, this type of PCS display provides a general knowledge of the local atmospheric conditions in a NWP region, in relation to current sensor altitude placement and location. Generally, large-scale surface ducts (> 50 m) should be an indicator that further investigation may be warranted, by performing a more detailed RF performance assessment.

4.3 EVAPORATION DUCT HEIGHT

Figure 9 shows a special case of the surface duct PCS display, in that only contours of evaporation duct height are shown. Evaporation ducts are ubiquitous over the oceans, and their effects are frequency dependent. In this display, the significant impact occurs for surface-based emitters operating at frequencies of 2 GHz and higher, as noted in the narrative below the contour display.

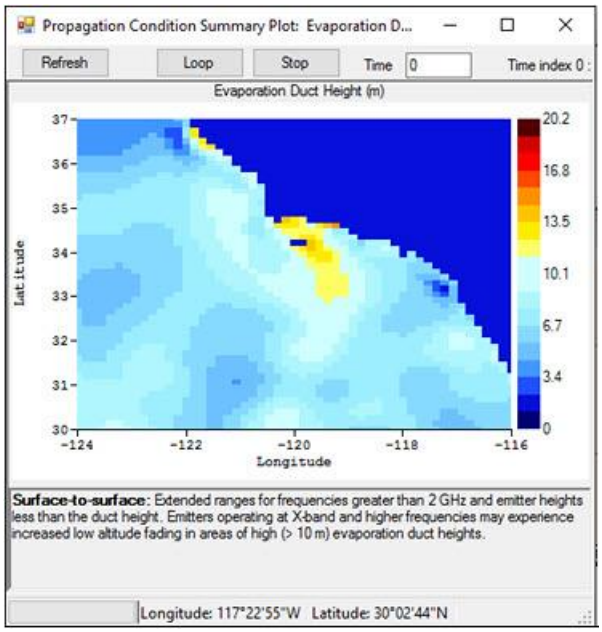

Figure 9 Evaporation duct height PCS display.

4.4 EXTENDED RANGE MAP – AIRBORNE EMITTERS

Similar to the extended range map for surface emitters, the extended range map for airborne emitters displays areas where elevated ducts are present. Due to the spatial horizontal and vertical extent of elevated ducts, this display comprises three graphics, where each must be viewed in combination with the other two. For instance, in Figure 10, the top two graphics illustrate the bottom (left) and top (right) of all elevated ducts present in the region. The bottom plot shows contours of the duct thickness, which is the difference between the duct top and bottom.

It could be argued that only two of the three graphics are necessary, as the third can be inferred from the other two. However, the general idea is to illustrate “at a glance” all anomalous conditions that can significantly impact propagation. As an example, the area marked “A” shows a large duct thickness, with low duct bottom and high duct top heights; one can immediately interpret this as a desired area for long range air-to-air communications, but high risk for long-range aircraft detection. Alternatively, viewing only the duct top graphic can aid in establishing a minimum flight altitude for aircraft to avoid long-range detection within the region altogether.

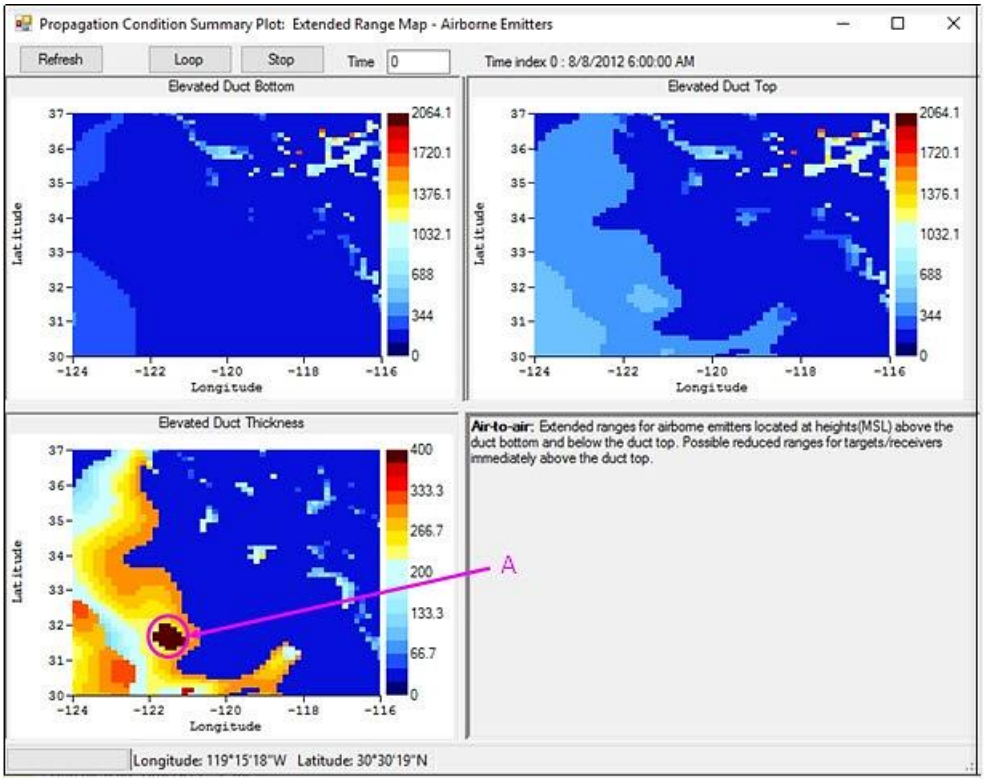

Figure 10. Extended range map - airborne emitters PCS display. Top (left) displays contours of the height of the elevated duct bottom; top (right) displays contours of the height of the elevated duct top; bottom (left) displays contours of the thickness of the elevated duct.

4.5 MINIMUM TRAPPED FREQUENCY/MAXIMUM TRAPPED WAVELENGTH

This PCS display is suitable primarily for communications applications. The presence of ducting features will imply that RF emitters *may* be subject to enhanced propagation if the antenna heights are within the duct. However, this condition is insufficient for enhanced propagation, as the ability of a duct to effectively trap RF emissions beyond the horizon is a function of the RF wavelength as well as the refractivity gradient and duct thickness (ITU-R, 2015). The minimum trapped frequency is the minimum frequency needed for RF coupling within the duct to produce enhanced propagation. Similarly, the maximum trapped wavelength is the largest wavelength that can be effectively trapped and undergo long-range propagation.

A word of caution should be made here in assuming that no enhanced propagation occurs if operating at a frequency below the minimum trapped frequency (or above the maximum trapped wavelength). The concept of “minimum trapped frequency” does not represent a cutoff frequency (or cutoff wavelength), but represents the minimum frequency at which *efficient coupling* of the RF energy within the duct occurs. At frequencies below the minimum trapped frequency and beyond, RF energy leakage continually increases until the duct’s impact is negligible. Therefore, at frequencies immediately below the minimum, you may still expect somewhat greater-than-normal communication ranges.

The maximum trapped wavelength, in meters, is determined as

$$\lambda_{max} = \frac{2}{3} CD\sqrt{\Delta M},$$

where $C = 3.77 \times 10^{-3}$ for surface ducts and $C = 5.66 \times 10^{-3}$ for elevated ducts (Brooks, Goroch, and Rogers, 1999). D is the duct height in meters, and ΔM is the maximum M-unit difference within the duct. Subsequently, the minimum trapped frequency is $f_{min} = {}^{c_0}/_{\lambda_{max}}$, where c_0 is the speed of light. The displays provided here refer to surface ducts only, excluding the evaporation duct, to address typical shipboard communication frequency bands. The evaporation duct is a special case within this category as enhanced propagation occurs at all frequencies above 2–3 GHz, regardless of duct height.

Figure 11 displays contours of the minimum trapped frequency (left graphic) and maximum trapped wavelength (right graphic) over the same NWP region as in Figures 7–10. The displays, combined with the narrative, are again intended as a qualitative "quick look" to easily identify areas with potential for extended communications ranges and conversely, those areas at high risk for signal intercept.

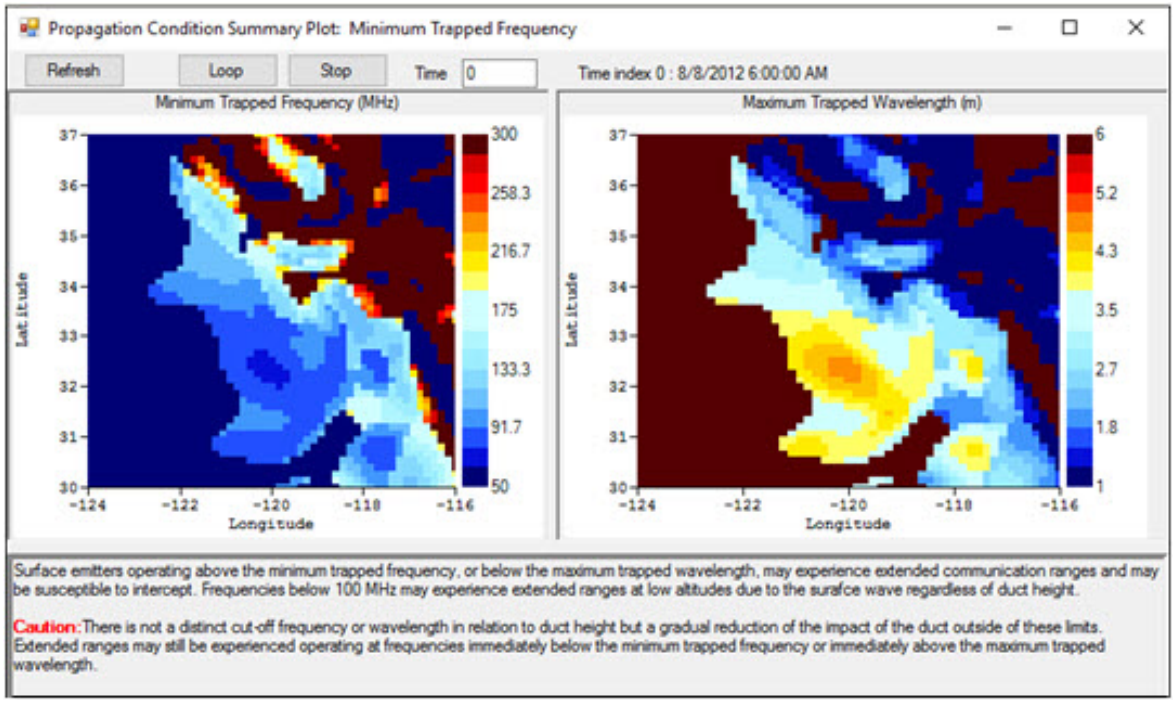

Figure 11. Minimum trapped frequency (left) and maximum trapped wavelength (right) PCS display.

5. HISTORICAL RF PERFORMANCE DATABASE

Part of the RFPPAS effort includes generation of a historical RF performance database, consisting of propagation loss predictions based on evaporation duct profiles computed from surface layer climatological statistics. The impetus for building such a database is to provide a means for instant generation of performance assessments based on environmental information that is relatively static and historical observation-based environmental information. This information would provide a simple means to conduct long [temporal] range mission planning over various geographical areas where surface layer climatology exists, as well as conduct quick RF assessments where in-situ or NWP environments are unavailable.

The current evaporation duct climatology (EDC) database incorporated in the AREPS was developed by NPS, and is computed from the Climate Forecast System Reanalysis (CFSR) dataset from 1979-2010 (http://www.esrl.noaa.gov/psd/data/reanalysis/reanalysis.shtml). The EDC was computed using the Navy Atmospheric Vertical Surface Layer Model (NAVSLaM), also developed by NPS (Frederickson, 2016). So far, the EDC statistics have been generated for only eight geographic regions, with more to come in future years. The regions are shown in Figure 12. Here the color contours represent mean evaporation duct height indicated by the color legend.

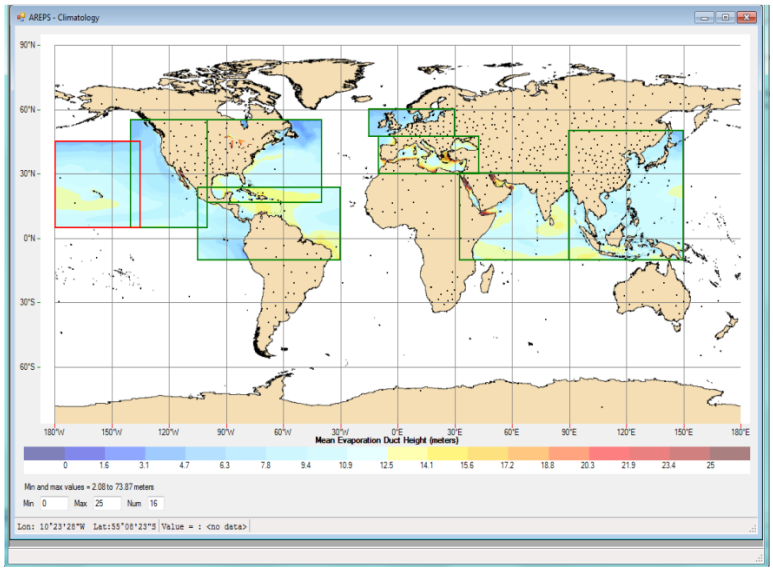

Figure 12. AREPS surface layer (evaporation duct) climatology regions.

Surface-based emitters, operating at roughly 3 GHz and higher, are most affected by evaporation ducts, therefore it is for these frequencies and geometries that propagation loss is determined for development of the database.

5.1 REFRACTIVE ENVIRONMENT

The refractive environment generated for the RF historical performance database is a merging of profiles of temperature, pressure and humidity (PTH) from the surface to a height of 20 km, the lowest 100 m from NAVSLaM with surface information from the EDC, and the upper air profiles from the National Center for Environmental Prediction (NCEP) Reanalysis (http://www.esrl.noaa.gov/psd/data/gridded/data.ncep.reanalysis.html). The EDC is a database of percentiles of surface and

surface-air properties, each with different spatial resolution. From the EDC, the median values for surface properties for 1200Z are used to generate PTH profiles from the NAVSLaM (v1.2) up to 200 m. The PTH profiles for the atmosphere up to 20 km are generated from a 40-year climatology from the NCEP Reanalysis, which is a globally uniform dataset with 2.5° resolution.

To merge these two datasets we need to horizontally interpolate and blend the two sets of PTH profiles. The NCEP profiles are interpolated to each location of the duct climatology database. The final profiles of PTH have three regions: the evaporation-duct-only region, the blended region, and the NCEP-only region. The evaporation-duct-only region uses the PTH profiles from NAVSLaM-generated EDC data, up to 100 m, with heights from 100–200 m used only for the blended region. The purpose of the blended region is to smoothly transition from the evaporation duct to the upper air region, without introducing sharp gradients that will significantly impact propagation calculations. To increase the region over which the blending occurs, the evaporation duct profiles are extended to 500 m, which is done by maintaining the gradient at the top of the PTH profiles generated by NAVSLaM. At heights from 100 to 500 m is then the blending region, and the blending is done independently in pressure, temperature, and humidity. We use a sinusoidal weighting function to further smooth the transition regions, especially near the top and base of the blending region. For the NCEP-only region, from 500 m to 20 km, the PTH profiles are taken directly from the NCEP climatology. Figure 14 shows an example grid point location within the Mediterranean climatology region, along with refractivity and gaseous attenuation rate profiles generated based on the scheme just described.

From the blended PTH profiles, profiles of modified refractivity and gaseous attenuation are calculated, the latter for frequencies from 3 to 35 GHz. Since the evaporation duct statistics exist for over-water areas only, all range-dependent refractive profiles are determined on over-water locations, limiting the propagation loss computation up to, but excluding, land areas.

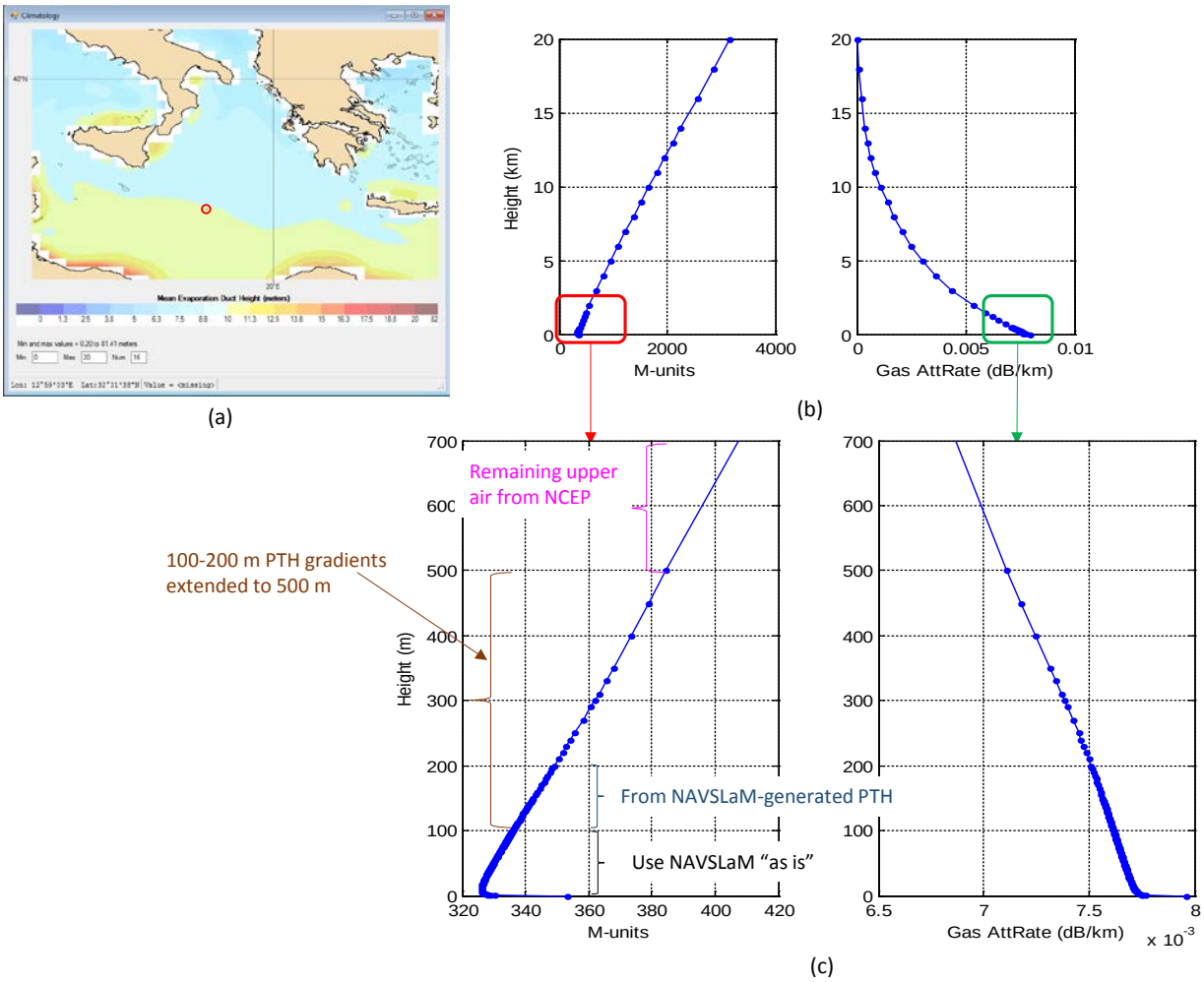

Figure 13. (a) Grid point location and mean ED height from the EDC for the sample profiles in (b). (b) Refractivity and gaseous attenuation rate profiles generated from EDC data located at the grid point in (a). (c) Lowest 700 m of profiles in (b) with ED-only, blending, and upper air regions.

5.2 COMPUTING PROPAGATION LOSS

The propagation model used to determine all propagation loss values is the APM. The specific frequencies, transmitter antenna heights, target heights, ranges, and other parameters required for the APM are listed in Table 7.

Table 7. APM inputs used for generation of the RF historical performance database.

Parameter	Value(s)	
Frequencies (GHz)	3, 5, 10, 15, 18, 20, 25, 30, 35	
Vertical and horizontal beamwidths	1.75°	
Elevation angles	0.0°, 0.75°, 1.5°, 2.25°, 3.75°	
Transmitting antenna pattern	Sinc(x)/x	
Polarization	Vertical, Horizontal	
Maximum range	475 km (256 nm) for 3 and 5 GHz, 200 km (108 nm) for all other frequencies	
Maximum height	10,000 m (≈32,800 ft)	
Transmitter antenna heights		
	13.7	45
	15.2	50
	16.7	55
	22.9	75
	24.4	80
	25.9	85
Receiver, or target, heights *(Nominal altitude for representative target)*		
Periscope	1.0	3
Small boat (pleasure craft, RHIBs, missile)	3.0	10
Medium boat (yachts, sailboats)	8.0	26
Ship – cruisers, DDGs	15.0	50
Ship – CVNs, LHAs, LHDs	23.0	75
Helicopters, UAVs	100.0	328
Small aircraft (2-4 person)	1,000.0	3,280
Jets, UAVs	4,500.0	14,700
Commercial aircraft	10,000.0	32,800

The generation of propagation loss within each climatology region is as follows:

1. The emitter is effectively placed at each over-water latitude/longitude grid point within the region.
2. From this location range-dependent refractive and gaseous attenuation rate profiles are determined along 36 azimuths at 10° increments according to the scheme described in Section 5.1. The profiles are determined out to the lesser of the maximum range for the prescribed frequency (in Table 7), or the first latitude/longitude location indicating land. Range-dependent surface winds are also included from the EDC.
3. For a given frequency, and at each azimuth, the APM is then executed for all elevation angles, emitter heights, and polarizations as provided in Table 7.
4. Propagation loss as a function of range for all receiver heights, listed in Table 7, are then stored in the database in binary format.

5.3 EXAMPLE APPLICATION

A simple example of one application of the historical RF performance (HRFP) database is shown in Figure 15. A naval vessel may wish to assess its X-band radar performance against small, low-flying aircraft in propagation conditions statistically relevant for the time and region. The top graphic

shows several latitude/longitude locations within the Mediterranean, labeled “1” through “4”, where the vessel may typically operate. Consider these grid points as representative of the vessel’s track. The pre-computed propagation loss, at X-band, for a target height of 100 m (328 ft) at these lat/lon locations are then extracted from the HRFP database. The propagation loss, shown in the bottom left four plots, is based on the range- and azimuthal-varying mean evaporation duct statistics for the month of March at the grid locations 1–4 out to 200 km. Once the loss is extracted we can easily determine the detection ranges for a nominal aircraft target RCS, which is shown in the lower right four plots. All range rings are at 40-km intervals. One can easily see there is a pervasive “skip zone” due to evaporation duct effects, with a shorter detection range of at least 10 km within the sector between 150° and 210° for the grid point labeled “3”. This is reflective of the range and azimuthal variation within the EDC database.

The computation time involved for this example is on the order of tens of minutes. However, we are considering only a few grid locations and a single frequency. When computing over the entire region for many variations of system parameters as listed in Table 7, the computation time can be prohibitive (on the order of hours to days). It is for this reason that the HRFP was created. Now, the climatology-based propagation loss can be retrieved instantaneously to satisfy many applications such as ship routing, radar or communications design, ship-to-shore communications planning, etc.

6. NEW CONCEPTS FOR VISUALIZATION OF RF PROPAGATION MODELING RESULTS

A final part of the RFPPAS effort was to conduct a preliminary investigation of new concepts in multi-dimensional data visualization, using virtual reality technologies. These visualization concepts were prototyped in collaboration with SSC Pacific’s Battlespace Exploitation of Mixed Reality (BEMR) Lab, and then partially demonstrated to Navy and civilian personnel during a visit to the Fleet Weather Center in Norfolk, Virginia.

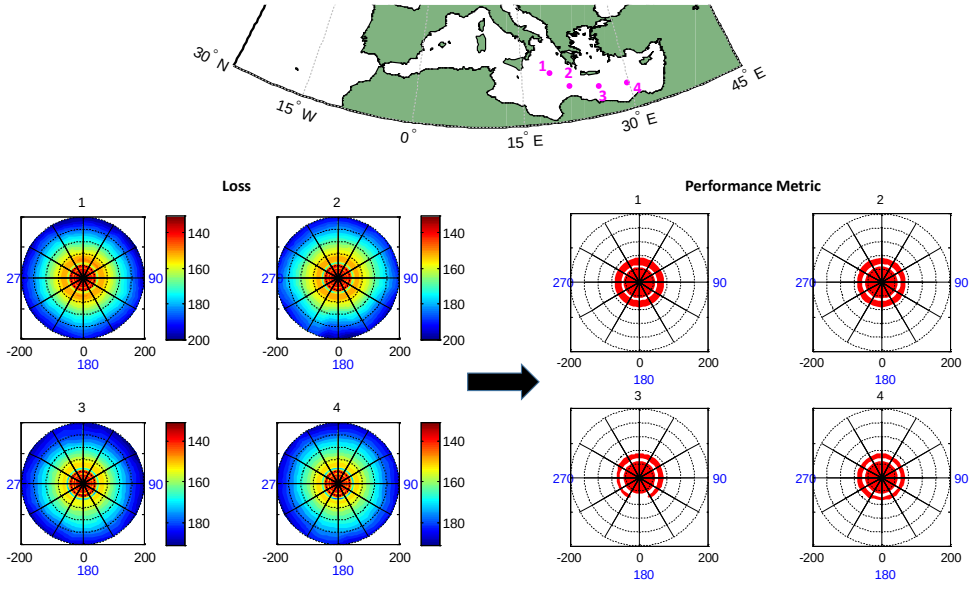

Figure 14. Example usage of the historical RF performance database.

6.1 INFORMATION DIMENSIONS IN RF PROPAGATION MODELING

A key component of any decision-support system is accurate information about the operating environment and relevant entities within it: their past, present, and predicted future. The system should allow the operator to manually find and inspect any element of that information, on demand. However, during regular semi-automated use as a decision support tool, the system should avoid showing too much information at once. Instead of information overload, it should selectively present the operator with the right information at the right time, in the context of the decisions, tasks, and overall mission threads being executed.

As shown on the left side of Figure 15, humans can readily interpret three dimensions at once in a "flat" 2-D graph + additional value. Animation can then allow the inclusion of a non-simultaneous fourth dimension, as represented by the time slider at the bottom. This is the approach currently taken by the AREPS, as shown in Figures 1–3: two spatial dimensions, one value dimension, and (optionally) animation of time or bearing. For example, the AREPS diagrams shown in Figure 1 and Figure 3 choose standard X and Y dimensions (range and altitude), plus propagation loss (Figure 1), or altitude error (Figure 3) at each X-Y point. The operator must look to external labels, not shown in the figure, to identify the values of additional relevant dimensions (or categories of dimensions):

- Location (where in the world is the 0,0 point shown?)
- Bearing (does propagation loss look the same at all the bearings not shown?)
- Target Location (are we equally concerned about all target bearings and altitudes?)
- Forecast Time (when is RF propagation predicted to look like this?)
- Target Type (e.g., airplane vs. ship vs. missile?)
- Radar Characteristics (waveforms, elevation angles, RCS detection modes, etc.?)
- METOC conditions (normal vs. enhanced vs. shortened propagation?)

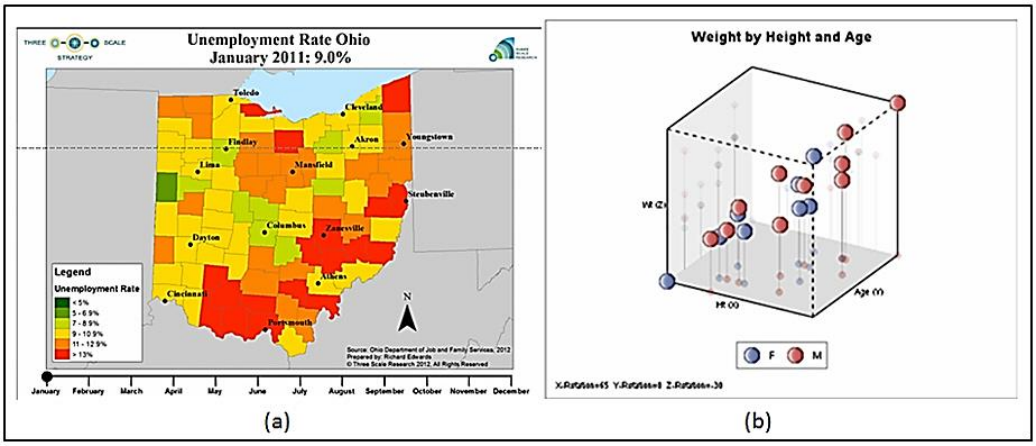

Figure 15. Two sample data visualizations (whose content is unrelated to this RFPPAS project). (a) An example of a clear simultaneous three-dimensional data visualization (latitude, longitude, and area classification). The inclusion of dataset time animation allows the addition of a non-simultaneous fourth-dimension (see "January 2011" in the title and the bottom slider). (b) An example of an unclear simultaneous four-dimensional data visualization (age, height, weight, and sex), demonstrating the problems of ambiguity and hiding. These interpretation problems are only partially mitigated by the inclusion of drop lines to the "floor" of the cube, side shadows on the left "wall" of the cube, and the ability to change viewpoint by rotating the data cube. Some mitigation attempts could even be said to make the interpretation problem worse, instead of better.

The AREPS coverage diagram shown in Figure 2a chooses a different pair of spatial dimensions from Figures 1 and 3: latitude and longitude. This handles the Location and Bearing questions that went unaddressed in Figures 1 and 3, but at the expense of omitting the Altitude dimension (now specified only by an external label, not shown in the figure); the remaining dimensional questions remain unspecified as well.

6.2 THE CHALLENGE OF MULTI-DIMENSIONAL 3-D+ DATA VISUALIZATION

Most decision support domains require operators to consider far more than three or four dimensions at once. The question then is how the system should support visualization of these dimensions by the operator. One approach is for the system to simply require the operator to pick three dimensions; any remaining integration with additional dimensions is left to the operator (unsupported). For example, in a standard AREPS coverage diagram, the "additional value" third dimension shown with range and altitude could be propagation loss (Figure 1), or altitude error (Figure 3), or probability of detection, but only one at a time. Integration across additional dimensions is left up to the operator.

Despite the use of only two spatial dimensions in the "flat" visualizations described above, realistic 3-D visualization is appealing to both users and system designers, since humans do live in a 3-D world. The problem is that going beyond the 2+1+1 method of visualizing four dimensions can encounter two difficulties, as seen on the right side of Figure 15:

- Ambiguity. From a high viewpoint looking downward, as in the example, a given data point could be high above a near X-Y point, or lower above a farther X-Y point, anywhere along the operator's line of regard into the data volume
- Hiding. Along the line of regard, data points can block the visibility of other data points.

Various methods have been employed to address these two issues, some of which are shown in Figure 15. These include supplemental labels, drop lines, wall shadows, data cube rotation (permitting a moveable viewpoint), and even allowing the user to "fly through" the 3-D dataset. These methods have met with limited success, in part because the 3-D dataset is still being shown as a 2-D projection (e.g., on a computer screen or on paper).

Several human factors research studies have compared human performance on command and control tasks using 2-D and 3-D displays. In a review of part of this literature, Smallman, St. John, and Cowen (2002) concluded that, "The experimental literature comparing 2-D and 3-D displays is large, complicated and contradictory, often showing mixed advantages for 3-D displays, at best. Users are better served by designers who consider the nature of the user's tasks and then tailor the display view, symbology, and depth cues to best suit those specific tasks."

6.3 3-D VIRTUAL REALITY (VR): GENERAL VISUALIZATION CHALLENGES

Virtual Reality (VR) involves a user experiencing a fully computer-generated visual environment while wearing a special headset with goggles. The 360-degree experience is immersive because the goggles dynamically and stereoscopically display the user's 3-D field of view into the environment, from the user's location, and in whichever direction the user turns the head to look. Controls then allow the user to move within the environment. By contrast, Augmented Reality (AR) involves computer-generated imagery overlaid onto an actual scene, for instance via special glasses, a cockpit heads-up display, or a handheld tablet that augments live video of an object . AR imagery can be "attached" to the environment ("augmenting" a real-life object), or attached instead to the viewer (moving with the environment, as the viewer's location or viewing angle changes). It is therefore possible to combine AR into VR, or to display AR alone. This project primarily investigated VR, although AR features (such as a floating compass and control panel) were also implemented.

The human visual system is finely tuned to make depth and distance judgments based on a variety of visual cues. Since the RFPPAS data set to be visualized was 400 nm wide, care had to be taken to minimize visual cues that would be inconsistent with that scale. For example, Figure 16 shows a VR scene of a 200 nm-radius circle over open ocean; nighttime was chosen to avoid the problem of showing size-realistic daytime clouds. Similarly, the particular VR environment used allows the configuration of an ocean swell; to make that swell size as realistic as possible, its amplitude was set as low as could be distinguished from dead calm. Finally, the ship at the center of the circle could not be rendered as a recognizable ship without appearing to be many miles long, so a sphere was used instead.

VR is often used immersively to display a static scene for entertainment or training. For example, the user can virtually experience the interior of a room or vehicle, or can stand at the landing signals officer (LSO) console on the deck of an aircraft carrier to interact with virtual controls and equipment. In contrast, this effort examined the possibility of using VR for multi-dimensional data visualization. In particular, VR has the potential to provide the intuitive benefits of spatial 3-D visualization, including "flying around" to explore a dataset, while also addressing the ambiguity and hiding problems.

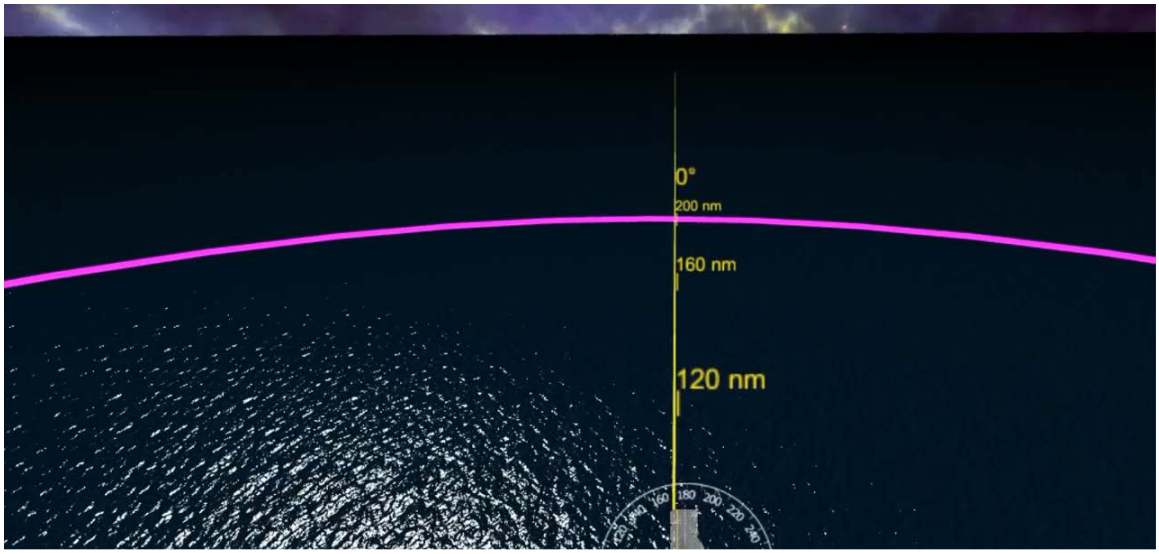

Figure 16. A 3-D/VR scene at night, looking down (steeply) to the north (0°), from within a 200-nm-radius circle (purple) around the location of the modeled ship. Part of a floating gray "compass" is also visible at the bottom.

As shown in Figure 17, 3-D data visualization can be completely unworkable if done poorly. The data interpretation problems of ambiguity and hiding can be severe, when too much information is presented at the same time (see also the difficulty of interpreting Figure 5 above). Clearly, the answer is not to simply show 360 side-view coverage diagrams at once, like "cake slices," or multiple top-down coverage diagrams like Figure 3a at once, like a layer cake. Both problems can be entirely avoided, as discussed in the following section.

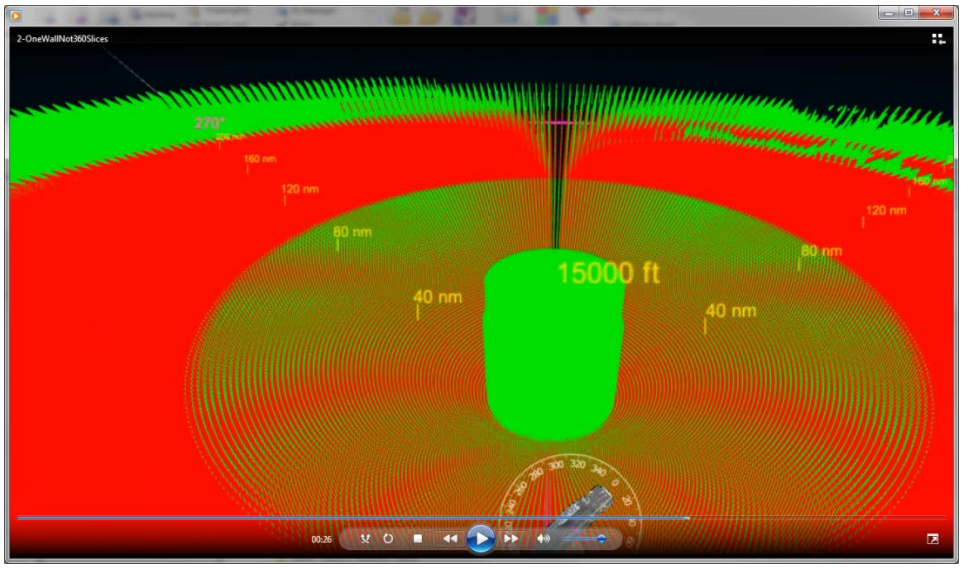

Figure 17. An ambiguity and hiding disaster: how not to usefully display data in 3-D/VR (360° range x altitude slices all shown at the same time, each an AREPS coverage diagram like Figure 1).

6.4 VR VISUALIZATION OF RF PROPAGATION MODELING RESULTS

To entirely avoid the 3-D problems of ambiguity and hiding, in this investigation only two non-overlapping slices were visualized at a time,180° apart from one another, forming a "data wall" (see Figure 18, showing the 266° slice and a bit of the 86° slice). Labels on the ocean surface provided scale and bearing information. Keyboard or virtual controls then allowed the user to rapidly sweep the data wall through other bearings, while the user's viewpoint was automatically swept in an orbit around the ship to maintain a perpendicular viewpoint to the wall. Other controls allowed the user to fly left/right/in/out/up/down to inspect the data wall without changing its bearings.

Figure 18 shows another improvement in intuitiveness over the standard AREPS coverage diagram. Whereas in Figure 1, a square representation shows a 540:1 horizontal compression (200nm wide and 2000 feet tall), here the scale of the altitude and range dimensions are more realistic. By being much less horizontally compressed, the visualization could aid intuitive understanding by the non-specialist of the RF propagation capabilities and limitations of the ship radar being modeled (a hypothesis that remains to be tested).

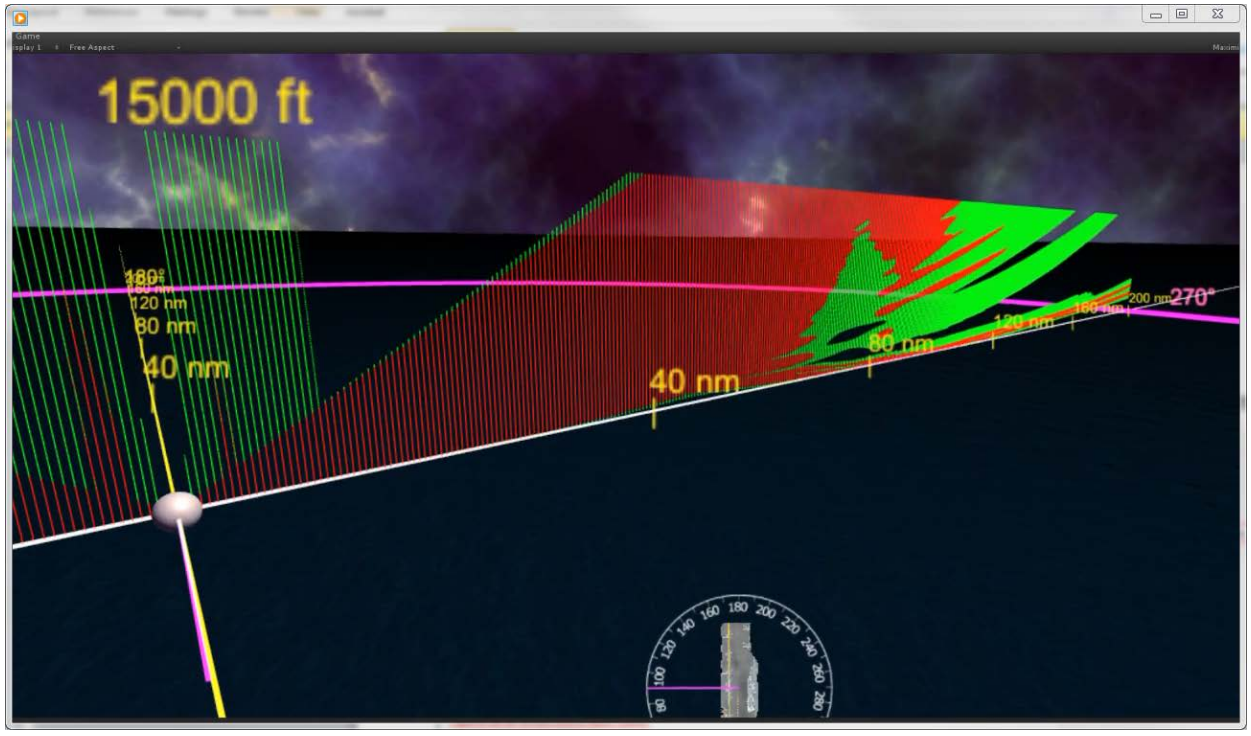

Figure 18. The "data wall": two AREPS coverage diagrams out of the available 360, each 180°apart from one another.

Floating AR labeling could then identify all the dimensional values of this particular modeling dataset, and controls could allow easy switching of this dataset with another dataset for ready comparison. This switching could provide a better way to handle the multi-dimensionality problem described above; the dataset switching could be in time (e.g., 4 vs. 8 hours from now), target type (e.g., airplane vs. missile), location (e.g., different potential courses of action for ship movement), and so on.

Figure 19 shows the power of VR to intuitively visualize the impact of current METOC conditions on RF propagation, as modeled by the RFPPAS. From the same RFPPAS dataset as Figure 18, but at bearing 348°, the user can see that ducting is creating a large "hole" in radar coverage. Theoretically, an adversary aircraft with knowledge of this hole could fly toward the ship along this bearing, and not be detected until it was about twice as close as it would have been on the bearing in Figure 18.

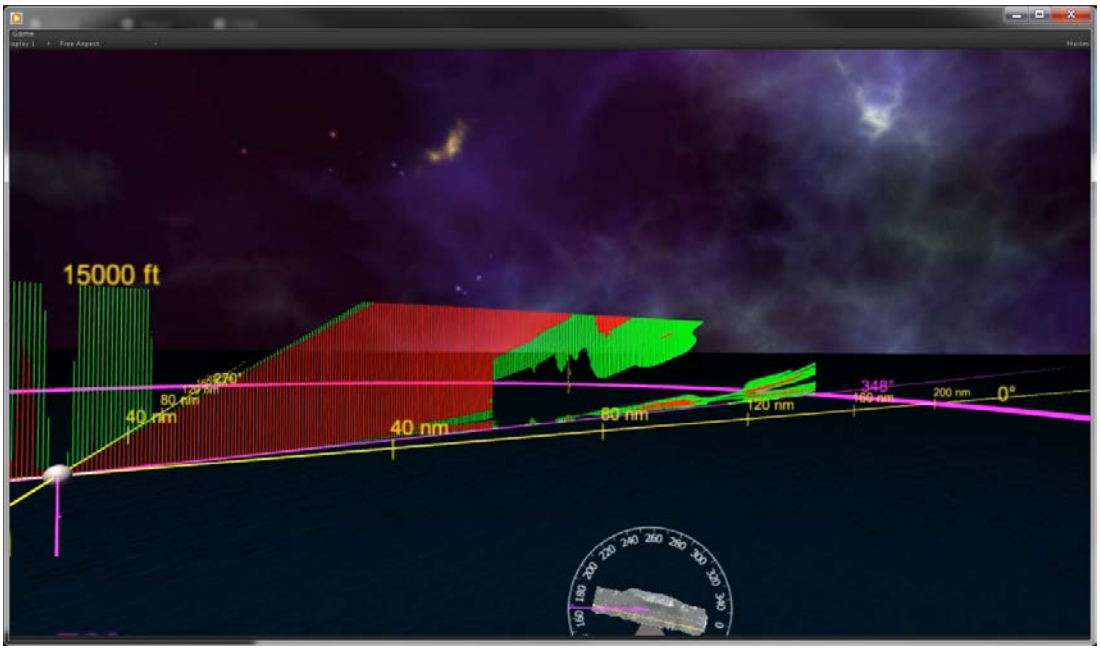

Figure 19. From the same dataset as in Figure 18, but at bearing 348°, a large radar coverage gap is apparent, potentially representing an increased vulnerability to the ship.

This investigation of data visualization with VR was very preliminary, and only points the way to additional research to investigate issues of usability and decision support effectiveness. Early prototypes were shown to Fleet users and civilian meteorologists at the Fleet Weather Center, Norfolk. Feedback was generally positive, despite the fact that technical limitations only permitted the demonstration in movie form rather than immersive and user-controllable VR form.

7. SUMMARY

The RFPPAS effort to modernize and "modularize" the underlying propagation model components within the AREPS now offers a means for easy distribution of these APIs and modules to be easily integrated into other programs of record, tactical decision aids, and system of systems. The primary transition target for the RFPPAS modules is PMW-120's NITES-Next PoR, however, the modules can be distributed and integrated into any application that requires the ability to perform RF propagation assessment. The "black box" design for the APIs and modules was done to ensure a standardized distribution, and a level of quality of control, of SSC Pacific's propagation modeling capabilities. This prevents the need to distribute source code which inherently carries the risk of unintended modifications and subsequent inconsistencies in RF performance results across various DoD applications.

8. REFERENCES

Barrios, A. 2016. “Advanced Propagation Model (APM) Implementation (Ver 5.2).” Prepared for SPAWAR Program Executive Office (PEO), Command, Control, Communications, Computers and Intelligence (C4I) Battlespace Awareness and Information Operations Program Office (PMW-120). March.

Barrios, A. In progress. “Improved Phased Array Radar Threshold Model with the Advanced Propagation Model (APM).”

Bilitza, D. 2001. “International Reference Ionosphere 2000.” *Radio Science* (March/April), vol. 36, no. 2, pp. 261–275.

Brooks, I. M., A. K. Goroch, and D. P. Rogers. 1999. “Observations of Strong Surface Radar Ducts over the Persian Gulf,” *Journal of Applied Meteorology and Climatology*, vol. 38, pp. 1293–1310.

Ferguson, J. A., and C. H. Shellman. 1993. “The High-Frequency Benchmark Propagation Program.” NRAD (now SSC Pacific) Technical Document 2608. Space and Naval Warfare Systems Center Pacific (SSC Pacific), San Diego, CA.

Frederickson, P. A. 201. “Software Design Description for the Navy Atmospheric Vertical Surface Layer Model (NAVSLaM) CSCI (Version 1.2).” Prepared for the Naval Oceanographic Office Systems Integration Division (May).

International Telecommunication Union-Radiocommunication. 2015., “Effects of Tropospheric Refraction on Radiowave Propagation.” Recommendation ITU-R P.834-7 (October).

Jones, R. M., and J. J. Stephenson. 1975. “A Versatile Three-dimensional Ray Tracing Computer Program for Radio Waves in the Ionosphere.” OT Report 75-76. Department of Commerce Office of Telecommunications. U. S. Government Printing Office, Washington, DC.

Lynch, S. 2014. “IonRayTrace: an HF Propagation Model for Communications and Radar Applications.” Technical Report 3286. Space and Naval Warfare Systems Center Pacific (SSC Pacific), San Diego, CA.

Patterson, W. L., C. P. Hattan, G. E. Lindem, R. A. Paulus, H. V. Hitney, K. D. Anderson, and A. E. Barrios. 1994. “Engineer's Refractive Effects Prediction Systems (EREPS) Version 3.0.” NRaD (now SSC Pacific) Technical Document 2648 (May). Space and Naval Warfare Systems Center Pacific (SSC Pacific), San Diego, CA.

Patterson, W. L., and A. Barrios. 2016. “Advanced Refractive Effects Prediction System (AREPS) v4.1 Help.”

Skolnik, M. K. 2008. *Radar Handbook.* 3rd ed. The McGraw-Hill Companies, New York, Chicago, San Francisco, Lisbon, London, Madrid, Mexico City, Milan, New Delhi, San Juan, Seoul, Singapore, Sydney, Toronto.

Smallman, H. S., M. St. John, and M. A. Cowen. 2002. “Human Factors of 3-D Perspective Displays for Command and Control.” Paper presented to the Shared Awareness track of the 2002 Command and Control Research & Technology Symposium, Monterey, CA.
Available online at http://dodccrp.org/events/2002_CCRTS/Tracks/Track_8.htm, http://www.dtic.mil/tr/fulltext/u2/a461058.pdf. Accessed November 9, 2016.

REPORT DOCUMENTATION PAGE

Form Approved
OMB No. 0704-01-0188

PLEASE DO NOT RETURN YOUR FORM TO THE ABOVE ADDRESS.

1. REPORT DATE *(DD-MM-YYYY)*	**2. REPORT TYPE**	**3. DATES COVERED** *(From - To)*
September 2016	Final	

4. TITLE AND SUBTITLE

Radio Frequency Propagation and Performance Assessment Suite (RFPPAS)

5a. CONTRACT NUMBER

5b. GRANT NUMBER

5c. PROGRAM ELEMENT NUMBER

6. AUTHORS

Amalia Barrios
Stephen Lynch
Neil Gordon
Earl M. Williams

5d. PROJECT NUMBER

5e. TASK NUMBER

5f. WORK UNIT NUMBER

7. PERFORMING ORGANIZATION NAME(S) AND ADDRESS(ES)

SSC Pacific
53560 Hull Street
San Diego, CA 92152–5001

8. PERFORMING ORGANIZATION REPORT NUMBER

TR 3043

9. SPONSORING/MONITORING AGENCY NAME(S) AND ADDRESS(ES)

SSC Pacific
Naval Innovative Science and Engineering (NISE) Program
53560 Hull Street
San Diego, CA 92152–5001

10. SPONSOR/MONITOR'S ACRONYM(S)

11. SPONSOR/MONITOR'S REPORT NUMBER(S)

12. DISTRIBUTION/AVAILABILITY STATEMENT

Approved for public release.

13. SUPPLEMENTARY NOTES

14. ABSTRACT

The Radio Frequency Propagation and Performance Assessment Suite (RFPPAS) is a 2-year effort funded under Space and Naval Warfare Systems Center Pacific's (SSC Pacific) Naval Innovation Science & Engineering (NISE) Technology Transition (TT) Program.

The objective of the RFPPAS project is to create thread-safe software modules and associated APIs from models and algorithms within the Advanced Refractive Effects Prediction System (AREPS). In a nutshell, the RFPPAS "cannibalizes" an operationally fielded tactical decision aid (TDA) for predicting radio frequency (RF) sensor performance, and then updates and improves its components to deliver fast, cloud-based, RF modeling performance on demand.

This software re-engineering effort will enable immediate integration of RFPPAS modules into PMW-120's program of record (PoR), the Naval Integrated Tactical Environmental System (NITES)-Next, as well as other new and existing software tools that rely on AREPS components. In addition, human-systems integration (HIS) and data management concepts were used to develop new databases and methodologies for creating decision aids, from large volumes of data and for multiple emitter/receiver(target) scenarios. Finally, a preliminary investigation was conducted into new concepts in multi-dimensional data visualization, using virtual reality technologies.

15. SUBJECT TERMS

Radio Frequency Propagation and Performance Assessment Suite (RFPPAS); Advanced Refractive Effects Prediction System (AREPS); tactical decision aid; thread-safe software modules; aplication program interface; multi-dimensional data visualization; virtual reality technologies; human-systems integration (HSI)

16. SECURITY CLASSIFICATION OF:			**17. LIMITATION OF ABSTRACT**	**18. NUMBER OF PAGES**	**19a. NAME OF RESPONSIBLE PERSON**
a. REPORT	**b. ABSTRACT**	**c. THIS PAGE**			Amalia Barrios
U	U	U	U	46	**19B. TELEPHONE NUMBER** *(Include area code)* (619) 553-1429

INITIAL DISTRIBUTION

84300	Library	(1)
85300	Archive/Stock	(1)
55280	A. Barrios	(1)
55280	N. Gordon	(1)
55280	S. Lynch	(1)
53603	E. M. Williams	(1)

Defense Technical Information Center
Fort Belvoir, VA 22060–6218 (1)

Approved for public release.

SSC Pacific
San Diego, CA 92152-5001